Chapter II

DEVIATIONS FROM IDEAL CONDITIONS

§13. FACTORS CAUSING DISTURBANCES AND SYSTEMATIC MEASUREMENT ERRORS

The conclusions derived from the general theory of aspiration counters are strictly valid only when the ideal conditions defined in the preceding chapter are fulfilled. In practice it is often impossible to fulfill all the conditions which lead to disturbances giving rise to systematic errors in the measuring results.

The danger of systematic errors forces us to focus our attention on the quantitative determination of these disturbances. Without such a determination it is impossible to judge whether or which disturbances appear under certain conditions. A quantitative evaluation of the disturbances is necessary for the proper choice of experimental parameters and observation methods.

More involved is the problem of applying the theory of the aspiration counter without allowing for one or another limiting requirement. The first step in the present book will be the determination of corrections eliminating the systematic errors due to small disturbances.

The measurement errors in the air-ion spectrum may be divided into three groups according to the nature of the disturbance source.

The first group comprises errors depending on the degree of perfection of the instruments employed for measuring the current, voltage, gas flow rate, etc., and errors due to the instability of the voltage supply, different contact potentials /Benndorf, 1909, 1926; Scholz, 1931a; Israël, Dolezalek, 1957/, etc. Some of these errors will be treated in Chapter III.

The second group comprises errors due to external conditions. Under ideal conditions the spectrum $q(k)$ at the counter inlet should be homogeneous and equal to the function $q(k)$ of the air sample. Deviations from this requirement may be caused by an external electric field, by a disturbance in the air movement at the measurement point, or by other factors. Of greatest practical significance is the electric field, which complicates the study of atmospheric air ionization /O'Donnel, 1952; Chalmers, 1953/. Information on the effect of the external electric field upon the measurement results may be found in a number of works /Swann, 1914d, 1923; Mackell, 1921, 1923; Norinder, 1921; Wait, 1934; Coroniti, Parziale, Callahan, Patten, 1952; Phillips, 1963; Ivanova, Kuklina, Sedunov, 1963; Zachek, 1964b; Schmeer, 1966/. The disturbance due to the external electric field may be eliminated by proper voltage regulation of the apparatus /Higazi, Chalmers, 1966/. The movement of air ions in the free atmosphere constitutes a problem which lies beyond the scope of this book, and we shall

therefore refrain from a detailed consideration of errors of the second group.

The present chapter deals with the errors of the third group which are caused by deviations from ideal conditions within the counter. The complexity of the problem compels us in most cases to consider small deviations in the first approximation. Neglecting the interaction of the disturbances, we shall be able to consider separately various deviations from the ideal conditions.

For various reasons we shall not discuss the interaction of certain disturbances of the third group. The problem of the unstable operation of the measuring capacitor is considered in detail in the works /Komarov, 1960a, 1960b/. The precipitation of air ions by inertial forces is of definite significance in conductivity measurements in clouds. This problem is dealt with in the works /Zachek, 1962, 1964a, b, 1965/. The disturbance due to inertial forces is removed in those counters having a modulated precondenser.

The effect of air-ion generation in the measuring capacitor on the measurement results is connected with the accumulation of radioactive substances on aerosols /Kurz, 1906, 1907/. The theoretical evaluation of this disturbance is involved and has so far not let to any definite results. In practice, the generation of air ions inside the measuring capacitor is determined directly from the current measurement for operating conditions corresponding to $\Phi = 0$. The effect of the radioactive substances precipitated on the plates depends basically only on the distance between the plates and increases with increasing distance. The effect of radioactive substances contained in air also depends on the distance between the plates but, in addition, is proportional to the filling time of the capacitor

$$t_0 = \frac{\pi l \left(r_2^2 - r_1^2\right)}{\Phi}. \tag{13.1}$$

Expression (13.1) applies to a cylindrical capacitor. For a parallel-plate capacitor we have

$$t_0 = \frac{lcd}{\Phi}, \tag{13.2}$$

where c is the width of the capacitor.

The disturbance due to radioactive radiation is suppressed in counters having a modulated precondenser.

The filling time of the capacitor also determines the effect of air-ion recombination in the measuring capacitor on the measurement results. The relative error in recombination and attachment of air ions to aerosol particles is limited by the inequality

$$\delta < \frac{t_0}{t_i}, \tag{13.3}$$

where t_i is the mean lifetime of the air ion. For light ions in the case of polar charge densities $t_i \approx \frac{600{,}000}{\varrho_\pm \text{ (el. charges/cm}^3\text{)}}$ (sec), where $\varrho_\pm$ is the charge density of air ions of opposite polarity.

The generation and recombination of air ions in the measuring capacitor may partly compensate one another. In the works /Vogler, 1959, 1960/ the

so-called "emission effect" is discussed. Upon decay the radioactive atom radiates α- and β-particles, the charges of which do not fully compensate one another. This gives rise to an additional current from the collector plate, upon which the radioactive substances have accumulated. According to Vogler /1959, 1960/ this current causes a considerable measurement error. An elementary quantitative evaluation shows that this statement is not valid. The "emission effect" is apparently smaller by several orders of magnitude than the effect of air ionization due to the same α- and β-particles, and can thus be of no practical significance.

§14. THE EDGE EFFECT

The edge effect results when the fringing electric field of the counter interacts with the air ions which are drawn into the measuring capacitor.

The nature of the edge effect depends on the manner in which the voltage is applied to the plates of the measuring capacitor. We shall therefore consider the different ways of applying the voltage to the measuring capacitor.

In most counters the inner plate is the collector plate. Because of certain technical advantages the collector plate is maintained at a potential close to the earth's potential. The outer plate in this case has a potential $-U$ relative to the earth. To remove the electric field outside the counter the outer plate is surrounded by a grounded screen. The diverging of the electric field around the entrance of the outer plate may be avoided with the aid of a grounded entrance cylinder. An example of the entrance cylinder of such a measuring capacitor is shown schematically in Figure 14.1.

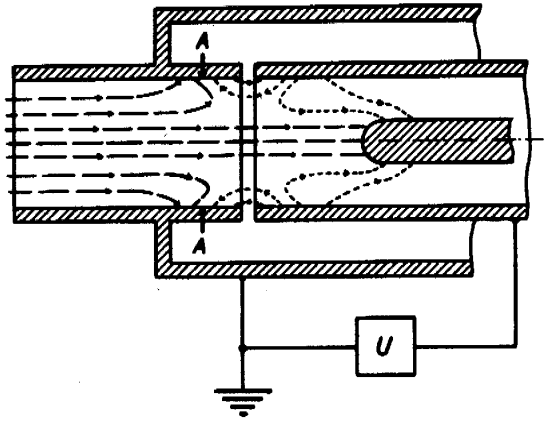

FIGURE 14.1. Example of a capacitor inlet:

– – – – – flow lines; · · · · · flow lines for which $\varrho(k) = 0$; A designates the separation region.

The edge effect in the above measuring capacitor may be analyzed from two equivalent points of view. First, if the entrance cylinder is not considered as a part of the measuring capacitor, then there exist no deviations from ideal conditions which could cause an edge effect. The edge effect is caused by the external electric field due to the potential between the outer plate and the entrance cylinder. In the second case the entrance cylinder may be considered as an additional plate of the measuring capacitor. The inlet of the measuring capacitor then corresponds to the inlet end of the entrance cylinder and the aspiration of the air to be studied will take place without any disturbances. The edge effect is the result of the settling of air ions on the plates of the inlet tube due to the influence of the electric field between the inlet tube and the external plate /Imyanitov, Zachek, In'kov, Semenov, 1960/. Both points of view are equivalent, but the latter is more convenient for theoretical quantitative calculations.

The first detailed description of the nature of the edge effect was given in /Lenard and Ramsauer, 1910/. The edge effect has subsequently been treated in a large number of works /Swann, 1914c; Itiwara, 1931; Scholz, 1931b, 1935; Gish, 1932; Israël, 1932a, 1932b; Graziadei, 1933/. The results of a detailed study on the nature of the electric fields occurring at the edge of various aspiration counters can be found in the work /Schmeer, 1966/. In his work /Israël, 1932a/ Israël proposed the quantitative theory of the edge effect—the so-called theory of the preliminary screening capacitor. According to this theory the edge effect becomes similar to the effect of the precondenser. The settling of air ions in the preliminary screening capacitor is calculated as in the case of the standard integral counter with a correspondingly small capacitance /Siksna, 1950; Israël, 1957b; Hoppel, Kraakevik, 1965/.

Let us consider the movement of the air ions of definite mobility near the inlet of the counter (see Figure 14.1). The spectrum $\varrho(k)$ at the inner surface of the inlet tube is either equal to the spectrum $\varrho_0(k)$ in the outside air, if the outward-emanating streamline of the air-ions terminates at the considered point, or to zero, if the streamline emanates from the external plate. Let us denote the mutual capacitance between the outer plate and that region of the inlet tube, where $\varrho(k) = \varrho_0(k)$, by C'. The capacitance C' depends, apart from the geometry of the electrodes, also on the location of the circle dividing the regions $\varrho(k) = \varrho_0(k)$ and $\varrho(k) = 0$ (Figure 14.1, A). If the location of the dividing circle would not depend on the operating conditions of the measuring capacitor, then the above considerations would validate the theory of the apparent precondenser. However, simple considerations show that the position of the dividing circle depends on the voltage and the air flow rate. This leads to a divergence from the known theory. When describing the edge effect, one may start with the concept of the apparent precondenser. However, the capacitance C' of the precondenser should be regarded as a function of the operation parameters of the counter. The expression for the G-function of the integral counter, taking into account the edge effect, is given by

$$G = \begin{cases} 4\pi CUk & \text{for} \quad k \leqslant k_0, \\ \Phi - 4\pi C'(U, \Phi, k)\,Uk & \text{for} \quad k_0 \leqslant k \leqslant k_0 \\ 0 & \text{for} \quad k_0 \leqslant k, \end{cases} \tag{14.1}$$

where the limiting mobilities are defined by the equations

$$k_0 = \frac{\Phi}{4\pi [C + C'(U, \Phi, k_0)] U}, \tag{14.2}$$

$$k_0' = \frac{\Phi}{4\pi C'(U, \Phi, k_0) U}. \tag{14.3}$$

Calculations according to the thus changed methods of the apparent precondenser lead to integral equations which cannot be solved in general form. This, along with the need to define initially the dependence of C' on the operating conditions of the counter, renders an exact quantitative determination of the edge effect difficult and compels us in most cases to restrict ourselves to an approximate determination.

There are counters which do not include a grounded entrance cylinder. Quantitative calculations are very involved because of the strong dependence of the edge effect on the movement of air in the vicinity of the counter and on other external factors. Generally, the character of the edge effect in this case should remain similar to that of the edge effect in counters with a grounded entrance cylinder.

Difficulties related to the edge effect required in many cases that the counter be connected in such a way that the potential of the outer plate is close to the earth's potential. As the collector plate one sometimes utilizes the inner and sometimes the outer plate. Let us first consider the counter with an inner collector plate, and the outer plate is grounded. If the counter is designed so that the inner plate is fully screened, then the air ions enter the measuring capacitor only under the influence of the air flow and the edge effect does not occur. The edge effect occurs only when the outer plate is too short and does not sufficiently screen the inner plate. In this case the electric field penetrates via the inlet into the outer space. The quantitative determination of the edge effect is difficult because of its dependence on conditions outside the counter. For a rough estimate we shall consider an approximate and simplified calculation /Tammet, 1962b/. Let us imagine a surface dividing the inner and outer space with respect to the measuring capacitor such that inside the counter the movement of air-ions proceeds in accordance with the assumptions in §2 and outside $\varrho(k)$ is uniform. There is no such surface in reality. Therefore, we shall tentatively choose an arbitrary surface at which deviations from the above-mentioned requirements are minimal. We shall seek the function G for the integral counter. Let us denote the mutual capacitance between the inner and outer plates as before by C and the capacitance of the edge effect, determining the flux of the electric field through the dividing surface, by C'. From considerations similar to those in §4 we obtain

$$G = \begin{cases} 4\pi(C + C')Uk & \text{for} \quad k \leqslant k_0 \\ \Phi + 4\pi C'Uk & \text{for} \quad k_0 \leqslant k, \end{cases} \tag{14.4}$$

where k_0 is expressed by formula (4.3). If in the corresponding ideal counter with active capacitance C the current is denoted by I_0, then we may write

$$I = I_0 + 4\pi C'U\lambda_{\pm}, \tag{14.5}$$

where $\lambda_{\pm}$ are the corresponding polar conductivities. Owing to the approximations used, (14.5) may serve only as a rough estimate of the errors caused by the edge effect. The application of this formula for the determination of corrections /Tammet, 1962b/ is not justified.

In counters with an outer collector plate the source of voltage is connected between the inner plate and ground. The potential of the outer plate is close to that of the earth. To prevent interference the counter is always screened. If the outer plate is sufficiently long in comparison to the inner one, then the counter with the outer collector plate will experience no edge effect. In the opposite case, an edge effect caused by the precipitation of air ions on the entrance tube occurs (Figure 14.2). The measuring capacitor of the integral counter is similar to that of the first-order differential counter with a divided capacitor and differs from it only by the quantitative ratio of the plate capacitances. This enables us to utilize formula (7.3) for the description of the edge effect. C_1 is the capacitance between the inner plate and the entrance tube and C_2 is the capacitance between the outer and inner plates. In practice the limiting mobility usually exceeds the mobility of the most mobile air ions. This simplifies calculations and the correction for the edge effect may be determined by the formula

$$I = I_0 - 4\pi C_1 U\lambda_{\pm}, \tag{14.6}$$

where I_0 is the current induced by the air ions in the corresponding ideal counter with active capacitance $C_1 + C_2$.

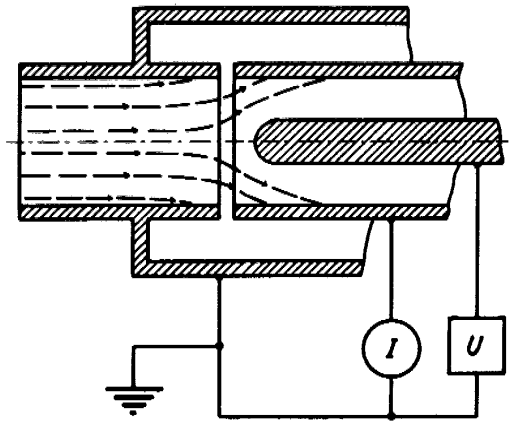

FIGURE 14.2. Edge effect in a counter with an outer collector plate.

If the counter is attached to a free balloon, then we cannot determine the way in which the counter plates are connected merely on the basis of whether the outer plate is grounded or not. No attention was given to the edge effect under these conditions /Kroenig, 1960; Mühleisen, Fischer, 1961/. A qualitatively correct description of the edge effect for the case of an isolated counter is given in the work /Schmeer, 1966/.

Neglect of the edge effect may be unjustified. The precipitation of air ions in the measuring capacitor charges the isolated system which may give rise to an edge effect similar to that in a counter, the outer plate of which is maintained at a certain voltage.

Consider a simplified example. Suppose a counter attached to a free balloon collects all the air ions from the passing air. If the space charge of the air is, for example, positive, then the apparatus acquires a positive charge Q. The charge Q may be expressed by the product of the apparatus capacitance C_s and the voltage $Q = C_s U_s$. This charge induces an edge effect which causes the current from the positive air ions measured by the counter to decrease by a value which is approximately proportional to the voltage U_s and the polar conductivity λ_+. We shall denote the decrease in the current generated by positive air ions by $4\pi C' U_s \lambda_+$, where C' corresponds to the capacitance of the edge effect. The apparatus will receive a current generated by negative air ions equal to $4\pi C_s U_s \lambda_-$. Assuming that the inner plate of the measuring capacitor is sufficiently screened by the outer plate, we obtain from the current balance condition the relationship

$$U_s = \frac{\Phi \varrho}{4\pi (C_s \lambda_- + C' \lambda_+)}, \tag{14.7}$$

where Φ is the air flow rate through the counter and ϱ is the space charge density. If the edge effect is not considered when measuring ϱ_+, we obtain the relative error

$$\delta = \frac{\varrho C' \lambda_+}{\varrho_+ (C_s \lambda_- + C' \lambda_+)}. \tag{14.8}$$

When measuring the current generated by air ions, the polarity of which is opposite to that of the space charge, the edge effect is not observed.

The edge effect does not affect the measurement results of polar conductivity obtained by means of the apparatus attached to a free balloon.

The above simplified example explicitly shows the nature of the edge effect in the case of an isolated counter. A more vigorous and general treatment of the problem will not be attempted. Because of the involved calculations this would hardly be of practical interest.

§15. RESULTS OF THE EXPERIMENTAL INVESTIGATION OF THE EDGE EFFECT

The problem of the edge effect is significant in the case when the outer plate of the measuring capacitor is maintained at a certain potential relative to the earth. To estimate the edge effect the capacitance C' must be known in each specific case as a function of the operation parameters of the measuring capacitor. The capacitance C' is preferably represented as a function of the similarity criteria. The flow field of air ions in the inlet section of the counter depends on the Reynolds number and the dimensionless number K_l, considered in §2. Below we shall use the following expressions for these criteria:

$$\mathrm{Re} = \frac{\Phi}{\pi \nu r}, \tag{15.1}$$

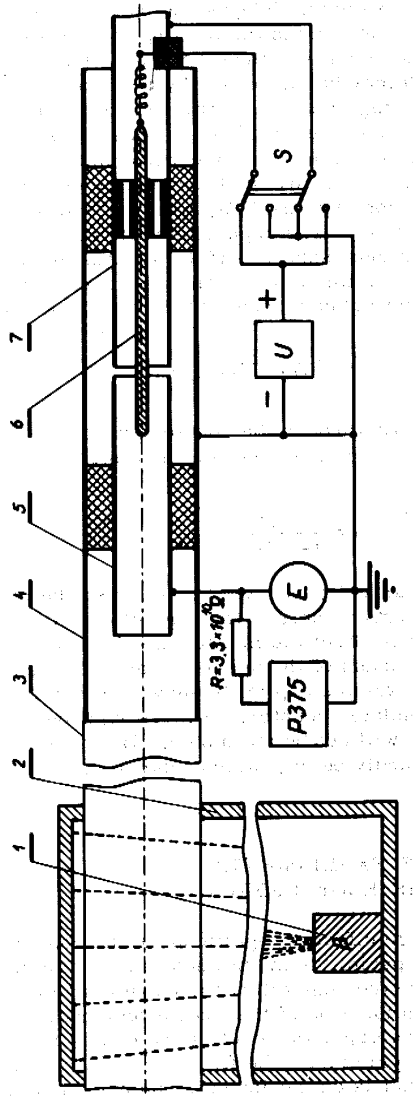

FIGURE 15.1. Arrangement for studying the edge effect:
1 – Sr^{90} preparation; 2 – chamber shielded against β-radiation; 3 – paper tube; 4 – cylindrical screen; 5 – first hollow cylindrical electrode; 6 – inner electrode; 7 – second hollow cylindrical electrode; E – electrometer (null indicator).

$$K_I = \frac{kr}{k_0 C} = \frac{4\pi Ukr}{\Phi}, \qquad (15.2)$$

where ν is the kinematic viscosity of air, r is the radius of the outer plate or the entrance tube (specified for each specific case), k_0 is the limiting mobility, C is the active capacitance of the measuring capacitor, U is the voltage between the outer plate and the entrance tube. The theoretical determination of the function $C' = C'(\mathrm{Re}, K_I)$ is difficult because of the laborious calculations, since the flow field of the air ions is determined only by numerical methods. Therefore, experiments were carried out with the aim of determining the capacitance of the edge effect of typical capacitor inlet units.

Experiments were performed with the aid of a device in which the electrode arrangement could be varied (Figure 15.1). Artificially ionized, unpurified laboratory air was used. In order to achieve a laminar flow, the air was drawn into the apparatus from a chamber having a volume of 0.1 m^3 through a special laminarizing arrangement (not shown in figure). The air ions were generated by β-radiation from the Sr^{90} preparation. The age of the air ions at the deposition point was about one second. Positive air ions, the mobilities of which were distributed over a narrower interval, appeared to predominate (Figure 15.2). The polar charge density was about 10^5 e.s.u./cm^3, which does not give rise to any appreciable disturbances. The current generated by the air ions was compensated by a current through a resistor (3.3×10^{10} ohm) connected to a precision potentiometer of the type P375; as a null-indicating device a dynamic recording electrometer was used to record the residual voltage. In this way an air-ion current instability of no higher than 0.2% was ensured. The decisive requirement for obtaining such a stability was the complete suppression of turbulence in the air-ion generation zone.

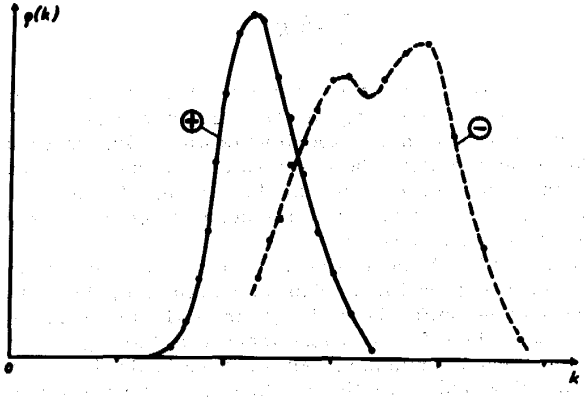

FIGURE 15.2. Spectra of positive and negative air ions according to measurement results obtained in § 21.

The geometry of the electrodes and the position of the switch S (Figure 15.1) correspond to the usual integral counter with an outer collector plate in which the edge effect does not occur. With the aid of such an arrangement the characteristic $I = I(U)$ of an integral counter, corresponding to the

constant active capacitance C, was determined. The measurement was performed by means of an ac bridge.

After turning the switch the edge effect current was measured. The first hollow cylindrical electrode, which previously served as the collector plate of the counter, now plays the role of the entrance tube and the second hollow cylindrical electrode becomes the outer plate. The direct measurement of the edge-effect current flowing to the entrance tube ensures greater accuracy than in the case of measuring the current through the inner plate of the counter. This is particularly important when the ratio of the edge-effect current to the saturation current is small. In order to alter the geometry of different entrance arrangements, exchangeable parts which could be placed on the electrodes were used. In a corresponding manner the geometry of the inner electrode was varied. The capacitance C' of the edge effect is calculated from

$$C'U' = CU, \qquad (15.3)$$

where U' is the voltage at which the edge-effect current equals the current generated by the air ions in the integral counter with an active capacitance C at a voltage U. Expression (15.3) is valid if all air ions have the same mobility. The dispersion of the air-ion spectrum smoothes the function $C' = C'(K_I)$, averaging out values of C' at neighboring points in accordance with the spectrum $\lambda(k)$. Such smoothing is essential only in the case of a strongly nonlinear behavior of the function $C' = C'(K_I)$, which is not observed in reality. The characteristics $I' = I'(U')$ of the edge effect were plotted for different values of the Reynolds number. The results are obtained in the form of the function $C' = C'(I'/I_0)$, where I' is the edge-effect current and I_0 is fluctuating current corresponding to the precipitation of all passing air ions. The parameter I'/I_0 is related to K_I as follows:

$$\frac{I'}{I_0} = \frac{C'}{r} K_I. \qquad (15.4)$$

The measurement results are shown in Figure 15.3 and the geometry of the corresponding entrance arrangements is given in Figure 15.4. The length of the entrance tube in all experiments was 9.5r. In Figure 15.3 the parameter I'/I_0 is plotted along the abscissa and the inclined straight lines correspond to the values of K_I shown in the figure. The errors due to the instrument itself and the instability of the current generated by the air ions range from one to several percent.

The decrease in C' with increasing K_I, for all entrance arrangements, is clearly evident in Figure 15.3. This is explained by the fact that an increase in the voltage shifts the dividing circle (Figure 14.1) toward the incoming air flow. The effective capacitance C' of the edge effect depends primarily on the Reynolds number. An increase in Re flattens the velocity profile of the air flow and shifts the dividing circle toward the outer plate. Even if the critical value of the Reynolds number is exceeded, the flow in the entrance arrangement will remain laminar; since in the wider tube of the air-ion generator the Reynolds number is less than the critical value and in the short entrance tube turbulence has no time to develop. Quantitative data on the dependence of C' on Re (Figure 15.3) are valid only for an entrance tube of length 9.5 r. For smaller lengths of the entrance tube the same values of C' are obtained for a smaller Re, and vice versa. The dependence of C' on the flow profile is clearly seen in curves 4 and 6,

corresponding to entrance arrangements with identical electrode geometry but differing from each other by the air-flow direction and the function of electrodes. A section consisting of a tube of smaller diameter was attached in one case to the first cylindrical electrode and in the other case to the second hollow cylindrical electrode (Figure 15.1). The inner electrode was removed. The air flow in the entrance arrangement in the first case diverges and in the second case converges. In the converging flow the velocity distribution is more uniform, causing larger values of C' than in the case of the diverging flow. In the asymmetric entrance arrangement, whereby the cross section of the entrance tube and the outer plate are equal (Figure 15.4 d without an inner plate), a similar change in the direction of the air flow and a change in function of the electrodes did not alter the effective capacitance within the limits of accuracy of the experiment.

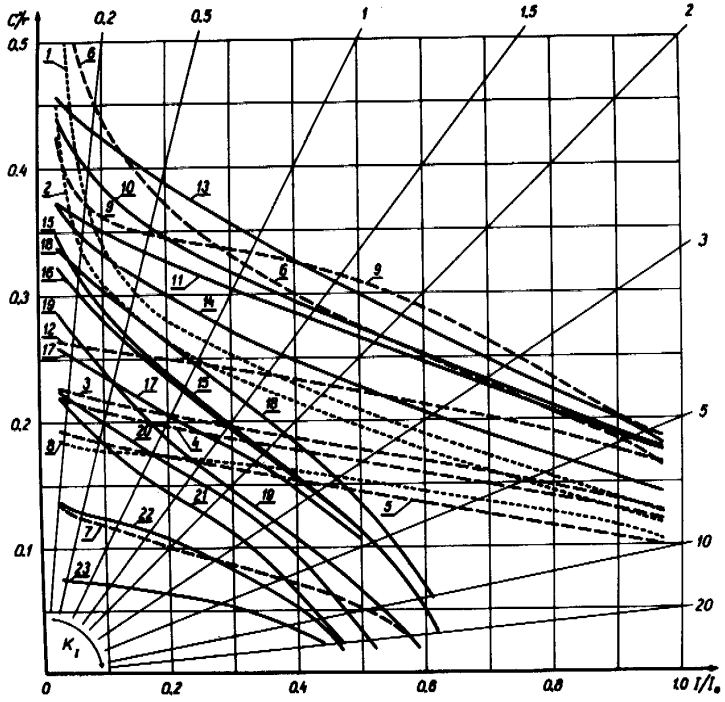

FIGURE 15.3. Edge-effect capacitance of different entrance arrangements. Below, the type of entrance arrangement (Figure 15.4) and the values of the parameters are listed according to the number of the curve:

1—c, Re = 2500; 2—c, Re = 250; 3—e, Re = 2500; 4—e, Re = 1000; 5—e, Re = 250; 6—e, with a reversed air flow, Re = 1000; 7—f, Re = 1000; 8—d, Re = 1000; 9— g, Re = 1000; values obtained from curve 9 should be doubled (the scale of curve 9 is halved); 10 —a, d/r = = 0.05 or d/r = 0.1 (results practically coincide), Re = 1000; 11—a, d/r = 0.2, Re = 1000; 12—a, d/r = 0.5, Re = 1000; 13—a, d/r = 0.1, Re = 2500; 14—a, d/r = 0.1, Re = 250; 15—b, d/r = = 0.05, r_1/r = 0.234, Re = 1000; 16— b, d/r = 0.1, r_1/r = 0.234, Re = 1000; 17—b, d/r = = 0.2, r_1/r = 0.234, Re = 1000; 18—b, d/r = 0.1, r_1/r = 0.234, Re = 2500; 19—b, d/r = = 0.1, r_1/r = 0.234, Re = 250; 20 = b, d/r = 0.1, r_1/r = 0.65, Re = 1000; 21—b, d/r = = 0.05, r_1/r = 0.83, Re = 1000; 22—b, d/r = 0.1, r_1/r = 0.83, Re = 1000; 23—b, d/r = 0.2, r_1/r = 0.83, Re = 1000.

Curve 8 in Figure 15.3 indicates that the entrance arrangement shown in Figure 15.4d used to eliminate the edge effect /Becker, 1909; Furman, 1960/ is ineffective, which was already convincingly pointed out earlier /Scholz, 1931b/. The edge effect is not removed, and is in fact increased when providing the entrance device with a grid (Figure 15.4g), which was erroneously proposed for the prevention of the edge effect /Imyanitov, Zachek, Inkov, Semenov, 1960/. This may be seen when comparing curves 9 and 10 in Figure 15.3. In the investigated device a grid with a mesh width of 0.15 r and a wire diameter of 0.034 r was used.

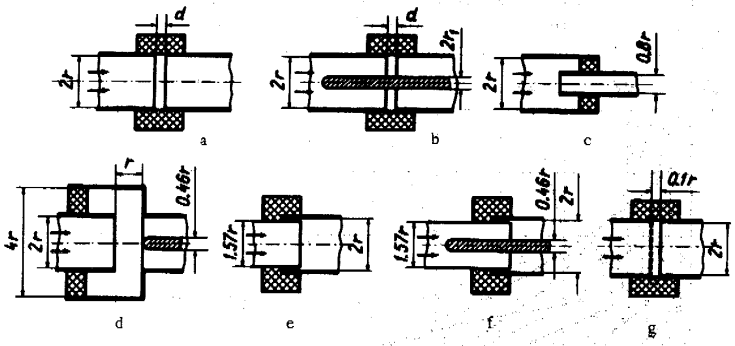

FIGURE 15.4. Entrance arrangements.

The edge-effect current of entrance arrangements f /Scholz, 1931b/ and b, in which the inner plate protrudes into the entrance tube, approaches some limit which is a certain fraction of the saturation current as the voltage is increased. This is reflected in the rapid decrease of C' when I'/I_0 approaches some limiting value (Figure 15.3, curves 7 and 15—23).

§16. EFFECT OF SPACE CHARGE ON MEASUREMENT RESULTS

The space charge of the air induces an electric field which may distort the electric field of the measuring capacitor. The electric field of the space charge causes an electrostatic dispersion of the air ions in the measuring capacitor.

Allowance for the distortion of the electric field of the measuring capacitor was made as early as 1906 /Franck, 1906; Becker, 1910/. The problem is considered in more detail in the work /Siksna, Metnieks, 1953; Siksna, Lindsay, 1961/. Here the intensity and the potential of the electric field in a cylindrical capacitor with a uniformly distributed charge density was calculated. In the first of the above works an error occurs which is corrected in the second work.

The effect of the space charge on the flow of air ions between the plates of the measuring capacitor is very complex. An attempt to calculate rigorously the effect of the space charge in the general theory of aspiration

counters does not give the desired results owing to the mathematical difficulties. When the charge density is large, the processes in the measuring capacitor acquire a nonlinear character and the function G starts to depend on $\varrho(k)$. An analytical solution of the counter equation is impossible and a numerical solution is not feasible because of the laborious calculations.

The piecewise-linear character of the function G, necessary for a simple solution of the counter equation, is retained if the distribution of the space charge between the plates of the measuring capacitor is uniform and does not depend on the operation parameters of the counter. Such a case will be considered in the present section /Tammet, 1962b, 1963a/. This is of some practical interest because the described situation may take place when measuring conductivities and studying the spectrum of light ions in air, the space charge of which is caused by heavy ions. The results obtained in the general case will suffice to obtain a rough estimate of the errors.

As a simplification, suppose that:

1) the measuring capacitor is an ideal cylindrical capacitor or an ideal parallel-plate capacitor;

2) the air flow field in the capacitor is uniform;

3) the charge density in the capacitor is distributed uniformly and does not depend on the voltage between the plates.

The charge Q of the collector plate is composed of the charge CU, dependent on the voltage between the plates, and the charge Q', induced by the space charge. We denote the equilibrium voltage of the collector plate by U'. If $U = U'$, then the charge $CU + Q'$ of the collector plate equals zero, and consequently $Q' = -CU'$, so that

$$Q = C(U - U'). \tag{16.1}$$

We can write the relationship

$$U' = a\varrho, \tag{16.2}$$

where a is a constant of the measuring capacitor.

To find the actual expression for the constant a, we must know the electric field of the measuring capacitor under the assumption $Q = 0$. The equation describing the electric field in a cylindrical capacitor has the form

$$\frac{1}{r}\frac{d(rE)}{dr} = 4\pi\varrho, \tag{16.3}$$

where r is the distance of the considered point from the capacitor axis. The solution of this equation for the boundary condition $E(r_1) = 0$ is

$$E_1(r) = 2\pi\varrho\left(r - \frac{r_1^2}{r}\right). \tag{16.4}$$

For the boundary condition $E(r_2) = 0$, we obtain

$$E_2(r) = -2\pi\varrho\left(\frac{r_2^2}{r} - r\right). \tag{16.5}$$

The voltage U' is determined by the integral of $E(r)$ over the interval (r_1, r_2). Calculating the corresponding integrals enables us to find the specific expressions for the constant a. In the case where the collecting electrode is the inner plate, we obtain

$$a = a_1 = \pi\left(r_2^2 - r_1^2 - 2r_1^2 \ln\frac{r_2}{r_1}\right). \tag{16.6}$$

In the case of the outer collector plate, the relevant expression is

$$a = a_2 = \pi\left(2r_2^2 \ln\frac{r_2}{r_1} - r_2^2 + r_1^2\right). \tag{16.7}$$

A similar calculation for a parallel-plate measuring capacitor yields

$$a = a_0 = 2\pi d^2, \tag{16.8}$$

where d is the distance between the plates.

The dependence of the constant a on the ratio of the radii of the plates of the cylindrical capacitor is shown in Figure 16.1.

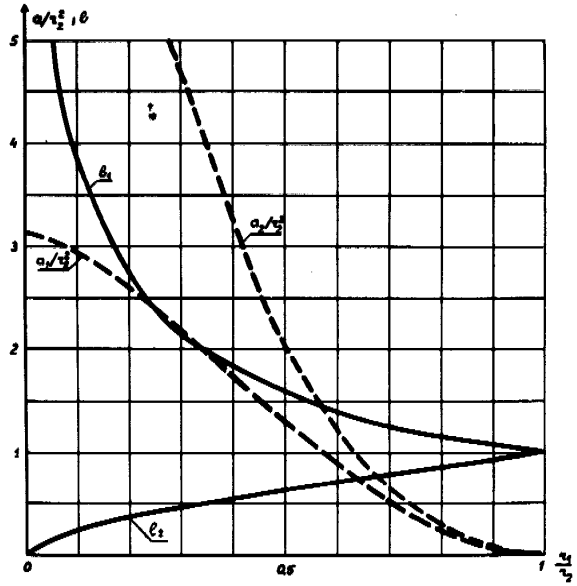

FIGURE 16.1. Dependence of the constants a and b on the ratio of the radii of the plates of the cylindrical capacitor.

Consider the behavior of a discrete group of air-ions with mobility k and partial charge density ϱ' in the measuring capacitor.

The variation of ϱ' with time is described by equation (2.10), which has, in the case of an unaltered charge density ϱ, the solution

$$\varrho' = \varrho_0' \exp(-4\pi\varrho k t), \tag{16.9}$$

where ϱ_0 is the initial value of ϱ' at the instant $t = 0$.

If ϱ' and Q have the same sign and the limiting surface does not intersect the second plate, then the function G can be found by integrating the current density $j' = kE\varrho'$ over the entire collector plate area and dividing the result by ϱ_0':

$$G = -kE\int\int_S \exp(-4\pi\varrho k t)\, dS. \tag{16.10}$$

t is the time required for the air ion to move from the beginning of the measuring capacitor to the point where it is precipitated. Denoting the distance from the beginning of the capacitor to this point by x, we obtain

$$t = \frac{x}{l} t_0. \tag{16.11}$$

We bear in mind the relationship

$$EdS = \frac{4\pi C(U - U')}{l}\, dx. \tag{16.12}$$

After integrating, we have

$$G = -\frac{C(U - U')}{\varrho t_0}\left[1 - \exp(-4\pi\varrho k t_0)\right]. \tag{16.13}$$

We shall introduce the concept of the characteristic mobility, defined by the expression

$$k' = \frac{1}{4\pi\varrho t_0}. \tag{16.14}$$

The characteristic mobility plays a similar role with regard to the electric field generated by the space charge as the limiting mobility with regard to the electric field induced by the voltage between the plates. Let us now write the function G for the entire interval of mobilities $(-\infty, \infty)$:

$$G = \begin{cases} 0 & \text{for} \quad k/k_0 \leqslant 0 \\ -4\pi C(U - U')k'\left[1 - \exp\left(-\frac{k}{k'}\right)\right] & \text{for} \quad 0 \leqslant k/k_0 \leqslant 1 \\ \Phi & \text{for} \quad 1 \leqslant k/k_0. \end{cases} \tag{16.15}$$

The limiting mobility k_0 is determined by the equality of the expressions of G in the interval $0 \leqslant k/k_0 \leqslant 1$ and $1 \leqslant k/k_0$:

$$-4\pi C(U - U')k'\left[1 - \exp\left(-\frac{k_0}{k'}\right)\right] = \Phi. \tag{16.16}$$

Eliminating k_0, we obtain

$$k_0 = k' \ln \frac{U - U'}{U + \left(\frac{t_0\Phi}{aC} - 1\right)U'}. \tag{16.17}$$

The term $t_0\Phi/aC$ is a dimensionless constant of the geometrical shape of the capacitor. To simplify the notation, we set

$$b = \frac{t_0\Phi}{aC} - 1. \tag{16.18}$$

It is easily verified that for a parallel-plate capacitor $b = 1$. For a cylindrical capacitor with an inner collector plate, we have

$$b = b_1 = \frac{a_2}{a_1} \tag{16.19}$$

and for an outer collector plate

$$b = b_2 = \frac{a_1}{a_2}. \tag{16.20}$$

The dependence of the constant b on the ratio r_1/r_2 is given in Figure 16.1.

Now that we have introduced b, we can express the characteristic mobility by

$$k' = \frac{\Phi}{4\pi CU'(1 + b)}. \tag{16.21}$$

We now write the formula for the limiting mobility

$$k_0 = k' \ln \frac{U - U'}{U + bU'}. \tag{16.22}$$

The last expression, notwithstanding its concise form, is inconvenient in the case of small U'/U-values. Although in the limit $U' \to 0$ the expression (16.22) transforms into the usual formula of the limiting mobility (4.3), a direct calculation is indeterminate. An evaluation of the errors arising when not allowing for the influence of the space charge is quite complicated. It is often more convenient to use the following expansion

$$k_0 = -\frac{\Phi}{4\pi CU}\left[1 + \sum_{n=1}^{\infty} \frac{\sum_{m=0}^{n} (-b)^m}{n+1}\left(\frac{U'}{U}\right)^n\right]. \tag{16.23}$$

For a parallel-plate capacitor this becomes

$$k_0 = -\frac{ud^2}{lU}\left[1 + \sum_{n=1}^{\infty} \frac{1}{2n+1}\left(\frac{U'}{U}\right)^{2n}\right]. \tag{16.24}$$

Considering the result obtained, it should be noted that the limiting mobility is indefinite in the interval $(U', -bU')$. In this interval the argument of the natural logarithm in the expression (16.22) has negative values and the series (16.23) and (16.24) do not converge. The dependence $1/k_0$ on U is shown in Figure 16.2. The behavior of k_0 is explained by the existence of a field strength inversion in the measuring capacitor if U is contained in the same interval. If $U=U'$, then the inversion layer reaches the surface of the collector plate; if $U=-bU'$, then it reaches the surface of the second plate. Since the air ions of any mobility cannot penetrate the inversion layer, there can be no limiting mobility for $U \in (U', -bU')$. If k_0 is indefinite, the function G has the form

$$G=\begin{cases} 0 & \text{for} \quad k/k' \leqslant 0 \\ -4\pi C(U-U')k'\left[1-\exp\left(-\frac{k}{k'}\right)\right] & \text{for } 0 \leqslant k/k'. \end{cases} \tag{16.25}$$

The equation of the counter is solved under the assumption $U \bar{\in} (U', -bU')$. We apply to the function G of the form (16.15) the modified operator h':

$$h'_U = 1-(U-U')\frac{\partial}{\partial U}, \tag{16.26}$$

which gives

$$h'_U G=\begin{cases} 0 & \text{for} \quad k/k_0 \leqslant 1 \\ \Phi & \text{for} \quad 1 \leqslant k/k_0 \end{cases} \tag{16.27}$$

From the last expression we obtain the formula for calculating the partial charge density:

$$\varrho(k_1, k_2)=\frac{h'_U I(U_1)}{\Phi_1}-\frac{h'_U I(U_2)}{\Phi_2}. \tag{16.28}$$

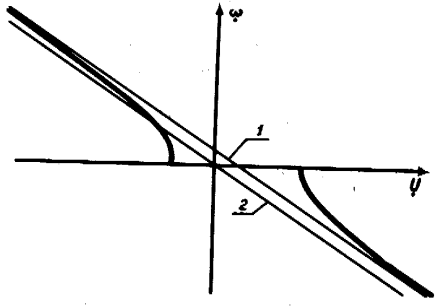

FIGURE 16.2. Dependence $\omega = 1/k_0$ on voltage: 1 – asymptote of the function $\omega(U)$; 2 – $\omega(U)$ for $\varrho = 0$.

The geometric interpretation of the operator h'_U is given in Figure 16.3.

The second derivative of the function G has the form

$$\frac{\partial^2 G}{\partial U^2}=-\frac{\Phi^2}{4\pi C(U-U')^2|U+bU'|}\delta(k-k_0). \tag{16.29}$$

Hence, we obtain the formula for the spectrum

$$\varrho(k_0)=-\frac{4\pi C(U-U')^2|U+bU'|}{\Phi^2}\frac{\partial^2 I}{\partial U^2}, \quad U \neq U'. \tag{16.30}$$

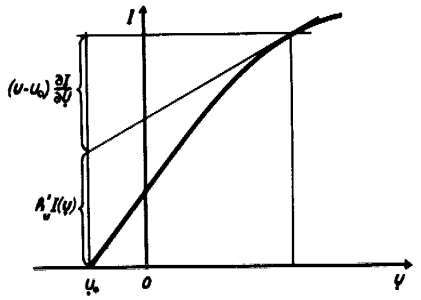

FIGURE 16.3. Determination of $h'_U I(U)$ by the method of tangents.

We note that all the above formulas were derived under the limiting conditions stated at the beginning of this section. If these conditions are not fulfilled, the results obtained merely suffice to effect a rough evaluation of the errors arising when not allowing for the space charge. Most characteristic of the distorting effect of the space charge is the error in the limiting mobility which can be conveniently estimated with the aid of the expansion (16.23). In the first approximation the error is determined by the absolute value of the first term of the sum

$$\delta'_k=\frac{|b-1|a\varrho}{2U}. \tag{16.31}$$

If the ratio of the radii of the plates of the cylindrical capacitor is small, we should consider also the second term which gives the correction

$$\delta''_k=\frac{(b^2-b+1)a^2\varrho^2}{3U^2}. \tag{16.32}$$

For a parallel-plate capacitor the error is expressed in the first approximation by

$$\delta'_k=\frac{4\pi^2\varrho^2 d^4}{3U^2}. \tag{16.33}$$

A simple computation shows that under conditions of natural atmospheric ionization, it is usually justifiable to neglect the effect of the space charge. The error in the limiting mobility becomes appreciable only in exceptional cases.

The effect of the space charge should always be accounted for in the case of artificial ionization. When designing a counter for measurement under

conditions of increased space charge density, it is useful to choose the smallest possible value for $r_2 - r_1$. As follows from (16.31) and (16.33) a decrease in the difference $r_2 - r_1$ enables an effective decrease in the counter sensitivity to the distorting effect of the space charge.

Additional errors arise from variations in the space charge density with time /Komarov, 1960a, 1960b/: A change in the charge density causes a variation in the induced charge Q'. The induced current is superimposed on the measured conduction current due to the air ions. A detailed calculation of the induced current is given in the works /Komarov, 1960a, 1960b/. Below we shall consider only the most simple case in which the space charge is induced by air ions, the mobility of which is considerably less than the limiting mobility. We can thus disregard the effect of the electric field of the measuring capacitor on the charge density. It should be noted that in this case variations in charge density present a serious problem, since the charge density may be of the same (or even larger) order of magnitude as the polar charge density of the precipitated air ions. When calculating the induced current, we start with the fact that the uniform space charge of the air filling the capacitor induces a charge $aC\varrho$ on the collector plate.

Taking into account the incoming as well as the outgoing charges, we obtain

$$I'(t) = \frac{aC}{t_0}[\varrho(t) - \varrho(t - t_0)], \tag{16.34}$$

where $\varrho(t)$ is the charge density at the beginning of the capacitor.

The error due to the induced current decreases as the current averages out with time and depends on the inertia of the recording instrument. The mean value of the induced current in the time interval Δt is

$$\bar{I}' = \frac{aC}{\Delta t}(\bar{\varrho}_1 - \bar{\varrho}_2), \tag{16.35}$$

where $\bar{\varrho}_1$ and $\bar{\varrho}_2$ are the charge densities between the plate of the measuring capacitor at the initial and final instants, respectively.

§17. MEASUREMENT METHODS BASED ON THE UTILIZATION OF THE ELECTRIC FIELD OF THE SPACE CHARGE

When the space charge density is appreciable, certain additional possibilities of measurement arise. For example, expression (16.2) points to the possibility of directly measuring the density of the space charge /Tammet, 1963a/. The voltage U' may be determined experimentally, since the potential of the insulated inner plate gradually approaches the value U'. The density of the space charge is calculated from the formula

$$\varrho = \frac{U'}{a}. \tag{17.1}$$

The above method for determining the charge density is similar to the well-known method of Thomson and may be considered as a modification thereof.

In the case of unipolar ionization the direct determination of U' involves large experimental errors. The equilibrium voltage of the inner plate may considerably exceed U' which is explained by the adsorption of ions. To prevent this U' should be determined by the extrapolation of the current intensity in the voltage interval $(U', -bU')$. The extrapolation is simplified by the fact that no limiting mobility exists in the indicated voltage range and the current intensity depends linearly on the voltage.

In many counters the current is determined from the accumulation of charge on the characteristic capacitance of the measuring capacitor. For such counters the following methods of practical determination of U' can be proposed. First, a rough intuitive estimation of U' is made on the basis of the observed voltage variation of the insulated inner plate. We choose a voltage U_1 which should be close to $-bU'$. Now we charge the inner plate to the potential U_1 or higher. We insulate the inner plate and determine the time Δt, which is the time required for the voltage to change from U_1 to 0. Then we follow the subsequent variation of the voltage and determine U_2, which is attained by the inner plate during the time interval Δt after passing through 0. U' is calculated in accordance with

$$U' = \frac{U_1 U_2}{U_1 + U_2}. \tag{17.2}$$

The derivation of this formula is based on a law whereby the voltage changes exponentially:

$$U = U'[1 - \exp(-\alpha t)], \tag{17.3}$$

where α is the unknown constant. Writing the corresponding expression for $t = -\Delta t$ and $t = \Delta t$, we obtain equations which can be solved by formula (17.2).

The above method of measuring the charge density widens the range of application of small-ion counters for the study of artificially ionized air. Under conditions of unipolar ionization it is possible for the small-ion counter to determine, apart from the partial density of small ions, also the partial charge density of large ions and even the mean mobility of large ions. The last quantity is calculated according to

$$\bar{k}(0, k_1) = \frac{\lambda(0, k_1)}{\varrho - \varrho(k_1, \infty)}. \tag{17.4}$$

Komarov /1960b/ developed a method in which the charge density is measured by a recording of the induced charge. The measuring capacitor is provided with a precondenser capable of collecting all air ions from the passing air. At the beginning of the measurement the voltage is disconnected from the precondenser and the main measuring capacitor is filled with a space charge. By measuring the induced charge $aC\varrho$, the charge density can be calculated. If the conductivity of the air is not too high and the induced charge is recorded by a low-inertia instrument, the diffusion of air ions does not constitute a negative influence in this method.

The last method of measuring the charge density can be combined with the earlier-described method of recording the equilibrium voltage. This

ensures the continuity of observations utilizing both the advantages characteristic of the method of equilibrium voltage and the rapid response characteristic of the method of induced charge. There is no need for a precondenser. This synthesis is possible owing to modern electrometers which effect compensation by means of feedback of the parasitic capacitance and render the effective capacity of the insulated system equal to the active capacitance of the measuring capacitor. In this case the voltage caused by the induced charge coincides with the equilibrium voltage. After switching on the instrument the insulated inner plate gradually acquires an equilibrium charge which then rapidly follows the variations in the charge density. However, along with the positive quality of the described arrangement, we must allow for the serious disadvantage caused by the effect of adsorption of air ions on the measuring results. The method is applicable if a sufficiently symmetric conductivity of the air sample can be assumed. To render the conductivity symmetric the air sample can be irradiated with radioactive radiation.

Tammet /1963a/ proposed a method for studying the air-ion spectrum based on the precipitation of air ions in the electric field of the space charge. The characteristics $I = I(\Phi)$ of the integral counter can be experimentally determined at $U = 0$. Because of limited applicability and the complexity in evaluating the observations this method is of no practical significance. Here, the manner in which the air-ion mobility is measured in the case when all air ions have the same mobility k may be of some interest. The equation of electrostatic dispersion then assumes the form

$$\frac{d\varrho}{dt} = -4\pi k\varrho^2. \tag{17.5}$$

The solution of this equation is

$$\varrho = \frac{\varrho_0}{1 + 4\pi k\varrho_0 t}, \tag{17.6}$$

where ϱ_0 is the value of ϱ at $t = 0$.

The current through the collector plate at $U = 0$ is calculated by integrating the current density over the surface area of the plate. In this case, we obtain

$$EdS = \frac{4\pi Ca\varrho}{l}\,dx, \tag{17.7}$$

hence the expression for the current may be written

$$I(0) = \frac{4\pi Cak}{l}\int_0^l \varrho^2(x)\,dx. \tag{17.8}$$

Integrating, we obtain

$$I(0) = \frac{4\pi Ca\varrho_0^2 kk'}{k + k'}, \tag{17.9}$$

where k' is determined correspondingly by the initial charge density. Eliminating k from the expression (17.9), we have

$$k = \frac{\Phi^2 I(0)}{4\pi CaI^*[I^* - (1+b)I(0)]}, \tag{17.10}$$

where $I^* = \varrho_0\Phi$ is the saturation current.

§18. THE ELECTRODE EFFECT

In still air, a space charge layer is formed in the vicinity of the charged electrodes which enhances the electric field strength at the electrode surface. This phenomenon may play a significant role in the aspiration counter if the air is sufficiently strongly ionized. Suppose that the density of the free space charge of the air sample equals 0 or is infinitesimal.

In the measuring capacitor the electric field separates the polar charges and consequently a layer of free space charge appears at both plates. The charge distribution in the measuring capacitor when measuring the conductivity is shown in Figure 18.1. Simple considerations lead to the conclusion that in this case the electrode effect is greatest. The determination of the electrode effect is in general involved. The problem is somewhat simplified when assuming a large limiting mobility because of the small thickness of the space charge layer in comparison to the distance between the plates. For simplicity, let us further suppose that the air contains positive air ions of mobility k_+ only and negative air ions of mobility k_- only.

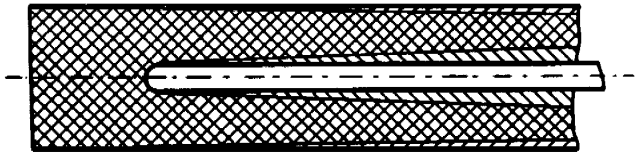

FIGURE 18.1. Distribution of charges causing the electrode effect. Hatching in one direction designates space filled with air ions of one polarity; hatching in the other direction shows the space filled with air ions of the opposite polarity.

The space charge in the vicinity of the surface of the inner plate induces an additional charge Q' on the latter. Since the charge of the inner plate in the absence of the electrode effect is $Q = CU$, the relative error in measuring the conductivity is

$$\delta = \frac{Q'}{CU}. \tag{18.1}$$

The induced charge Q' can be considered to be approximately equal to the charge in the layer of the space charge adjacent to the plate. The space charge formed on one plate primarily induces an additional charge on the same plate and only slightly affects the charge on the other plate. This

conclusion is readily verified with the aid of the well-known Ramo-Shockley theory.

To estimate the electrode effect the volume of the space charge layer must be calculated. This volume depends primarily on the velocity distribution of the air flow in the measuring capacitor. The hydrodynamic problem of air flow in a cylindrical capacitor has not been solved. The exact flow profile is known only for two boundary cases. In a potential flow the velocity distribution is uniform. For a high flow rate and a sufficiently short capacitor the air flow approaches a potential flow in the entire capacitor /Misaki, 1960; Hoegl, 1963b/. In a long measuring capacitor and for a low flow rate the flow approaches a steady laminar flow. The profile of the steady laminar flow is described by the formula /Lamb, 1947; Targ, 1951/

$$u(r)=\frac{2\Phi\left(\frac{r_2^2-r_1^2}{\ln\frac{r_2}{r_1}}\ln\frac{r}{r_1}+r_1^2-r^2\right)}{\pi\left(r_2^2-r_1^2\right)\left(r_2^2+r_1^2-\frac{r_2^2-r_1^2}{\ln\frac{r_2}{r_1}}\right)}. \tag{18.2}$$

Under intermediate conditions the actual flow differs considerably from the above two profiles. In this case more exact results are obtained when using the boundary layer theory.

If the conditions

$$\left.\begin{aligned}\sqrt{\nu t_0}&\ll r_2-r_1\\ \sqrt{\nu t_0}&\ll r_1\end{aligned}\right\} \tag{18.3}$$

are satisfied, the boundary layer at the plate is then similar to that at a flat plate. The flow velocity in the vicinity of the surface is /Loitsyanskii, 1959/

$$u(y)=0{,}332y\sqrt{\frac{u_0^3}{\nu x}}, \tag{18.4}$$

where y is the distance from the surface, x is the distance from the beginning of the plate and u_0 is flow velocity far from the plate.

When the air flow is potential, the calculation of the error δ is simple. The volume of the space charge layer at both plates is in the first approximation given by

$$V'=2\pi t_0 k_{\mp} CU. \tag{18.5}$$

Using (18.1), we obtain

$$\delta=2\pi t_0 k_{\mp}\varrho_{\pm}. \tag{18.6}$$

In these and in the following formulas the upper sign in the subscript will refer to the case $k_0>0$ (the voltage of the collector plate is negative), the lower sign to the case $k_0<0$ (U is positive).

In the center of the boundary layer the radial component of the flow velocity must be considered. To avoid mathematical difficulties we start

with the expression for the air flow rate through the dividing surface of the space charge layer which is defined in the first approximation by

$$\Phi'(x)=k_{\mp}N(x)=4\pi C(x)k_{\mp}U. \tag{18.7}$$

This expression describes the region of the surface of the space charge layer from the beginning of the plate to the point corresponding to the coordinate x. On the other hand, $\Phi'(x)$ is defined by (18.4):

$$\Phi'(x)=\pi r_c y u(y)=0.332\,r_c y^2\sqrt{\frac{u_0^3}{\nu x}}, \tag{18.8}$$

where r_c is the radius of the collector plate and y the thickness of the space charge layer at the point with coordinate x. From expressions (18.7) and (18.8) we can readily derive the equation for the surface of the space charge layer as follows:

$$y=2.46\left(\frac{k_{\mp}U}{r_c\ln\frac{r_2}{r_1}}\right)^{1/3}\left(\frac{\nu}{u_0^3}\right)^{1/4}x^{3/4}. \tag{18.9}$$

The volume of the space charge layer is given by the integral

$$V=2\pi r_c\int_0^l y(x)\,dx. \tag{18.10}$$

The expression for the error may be written in the form

$$\delta=2\pi t_0 k_{\mp}\varrho_{\pm}\sqrt{\frac{k_0}{k_{\mp}}}Y. \tag{18.11}$$

Actual calculations for the case of an inner collector plate yield

$$Y=Y_1=\sqrt[4]{\frac{780\nu l r_1^2}{(r_2^2-r_1^2)\Phi}} \tag{18.12}$$

and for the case of an outer collector plate

$$Y=Y_2=\sqrt[4]{\frac{780\nu l r_2^2}{(r_2^2-r_1^2)\Phi}}. \tag{18.13}$$

A similar calculation for the parallel-plate capacitor leads to the same formula (18.11), where

$$Y=Y_0=\sqrt[4]{\frac{62\nu l}{u_0 d^2}}. \tag{18.14}$$

The formulas obtained are applicable if the thickness of the boundary layer exceeds the thickness of the space charge layer. For the case of an inner collector plate the last condition is written as follows:

$$\left(\frac{k_0}{k_\mp}\right)^2 > \frac{(r_2^2 - r_1^2)\Phi}{4\pi r_1^2 \nu l}, \tag{18.15}$$

for the case of an outer collector plate

$$\left(\frac{k_0}{k_\mp}\right)^2 > \frac{(r_2^2 - r_1^2)\Phi}{4\pi r_2^2 \nu l} \tag{18.16}$$

and for the case of a parallel-plate capacitor

$$\left(\frac{k_0}{k_\mp}\right)^2 > \frac{u_0 d^2}{\nu l}. \tag{18.17}$$

The assumption of a steady laminar profile complicates the problem. However, the calculations can be simplified by the approximation

$$u(y) = \frac{du(r_c)}{dy}\, y, \tag{18.18}$$

since we are interested only in the thin layer of air in the vicinity of the plate. At the surface of the inner plate, we obtain

$$\frac{du(r_1)}{dy} = \frac{2\Phi\left(\dfrac{r_2^2 - r_1^2}{r_1 \ln \frac{r_2}{r_1}} - 2r_1\right)}{\pi(r_2^2 - r_1^2)\left(r_2^2 + r_1^2 - \dfrac{r_2^2 - r_1^2}{\ln \frac{r_2}{r_1}}\right)} \tag{18.19}$$

and at the surface of the outer plate

$$\frac{du(r_2)}{dy} = \frac{2\Phi\left(2r_2 - \dfrac{r_2^2 - r_1^2}{r_2 \ln \frac{r_2}{r_1}}\right)}{\pi(r_2^2 - r_1^2)\left(r_2^2 + r_1^2 - \dfrac{r_2^2 - r_1^2}{\ln \frac{r_2}{r_1}}\right)}. \tag{18.20}$$

Under the above assumptions the equation for the surface of the space charge layer is simply

$$y = \left[\frac{2k_\mp U}{r_c \ln \frac{r_2}{r_1} \frac{du(r_c)}{dy}}\right]^{1/3} x^{1/3}. \tag{18.21}$$

The calculation of the error δ leads to the formula (18.11) where Y for the case of an inner collector plate has the form

$$Y = Y_1' = \sqrt{\frac{32r_1\left(r_2^2 + r_1^2 - \dfrac{r_2^2 - r_1^2}{\ln \frac{r_2}{r_1}}\right)}{9(r_2^2 - r_1^2)\left(\dfrac{r_2^2 - r_1^2}{r_1 \ln \frac{r_2}{r_1}} - 2r_1\right)}}. \tag{18.22}$$

For the case of an outer collector plate

$$Y = Y_2' = \sqrt{\frac{32r_2\left(r_2^2 + r_1^2 - \dfrac{r_2^2 - r_1^2}{\ln \frac{r_2}{r_1}}\right)}{9(r_2^2 - r_1^2)\left(2r_2 - \dfrac{r_2^2 - r_1^2}{r_2 \ln \frac{r_2}{r_1}}\right)}}. \tag{18.23}$$

For a parallel-plate capacitor we obtain

$$Y = Y_0' = 0.77. \tag{18.24}$$

When estimating the electrode effect the conditions (18.3) and (18.15), (18.16) or (18.17) must first be verified. If these conditions are fulfilled, formula (18.12), (18.13) or (18.14) must be applied. In the opposite case, formulas (18.22)–(18.24) are used. Note that these formulas give the largest possible errors corresponding to a large limiting mobility. When k_0/k is small the errors are considerably smaller.

In the naturally ionized air of the air layer near the ground the electrode effect plays a significant role only in exceptional cases. The electrode effect constitutes a negative influence for stratospheric measurements. The possibility of distortions due to the electrode effect should always be taken into account when studying air with artificially produced ions of increased mobility.

To render the theory more rigorous the electrode effect and the effects of air-ion recombination should be simultaneously considered, since these distortions arise under the same conditions and may partly compensate one another. It is also advisable to allow for the electrostatic dispersion of air ions in the space charge layer.

§19. DIFFUSION OF AIR IONS

Diffusion is a consequence of the thermal motion of air ions which is of a random nature. The equation of motion $\vec{v} = \vec{u} + \vec{k}\vec{E}$, used in the preceding sections without reservations, is in fact merely the equation of the mean expected motion of the air ions. The actual trajectories of the air ions form a diverging beam about the mean trajectory defined by the above equation.

The first attempt to quantitatively estimate the effect of diffusion in an air-ion counter /Mache, 1903/ was unsuccessful because of erroneous

theoretical premises. In the work /Becker, 1910/ the starting principles and the qualitative characterization of diffusion are correct, but rough approximations used in calculations lead to serious disagreement with experimental data. More satisfactory is the evaluation of the random displacement of an air ion directly from formulas of the theory of Brownian motion /Zeleny, 1929/.

There are two methods which enable a mathematical description of the diffusion of air ions: the method of calculating the diffusion flow on the basis of the Fick equation and the statistical method used in the statistical theory of Brownian motion. The second method is the more appropriate for our purposes.

The influence of the diffusion of air ions in the measuring capacitor can be described in two ways. In the first case, the diffusion is already allowed for in the expression for the function G. The function G in this case loses its piecewise linear behavior (Figure 19.1), which complicates the solution of equation (3.3). In the second case, the effect of diffusion is represented as a transformation of the function $\varrho(k)$ into the function of the apparent distribution $\varrho^*(k)$, whereby the former trend of the function G is retained. The considerations below are based on this approach.

As a consequence of diffusion, an air ion of mobility k precipitates in the measuring capacitor at that point where, in the absence of diffusion, air ions of some other mobility k_1, which is the apparent mobility of the air ion under consideration, would precipitate. We shall denote the probability that an air ion of mobility k possesses an apparent mobility between k_1 and $k_1 + dk$ by $W(k, k_1)dk$. If the actual spectrum of air ions is characterized by the function $\varrho(k)$, then the apparent distribution is

$$\varrho^*(k_1) = \int_{-\infty}^{+\infty} W(k, k_1)\, \varrho(k)\, dk. \qquad (19.1)$$

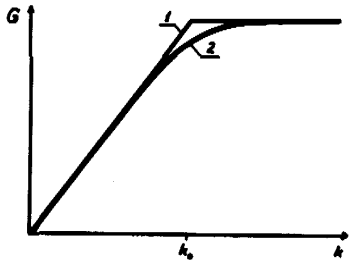

FIGURE 19.1. The function G of an integral counter:

1—ideal case; 2—when diffusion of air ions takes place.

The function $W(k, k_1)$ completely determines the effect of the diffusion of air ions on the measuring results. If this function is known, then formula (19.1) may be taken to define the actual spectrum $\varrho(k)$ on the basis of the

function $\varrho^*(k)$, calculated without allowance for the effect of diffusion. The solution of the integral equation (19.1) is rather involved. One is usually satisfied with the result $\varrho(k) \approx \varrho^*(k)$. The function $W(k, k_1)$ is used in this case only to estimate the errors caused when diffusion is disregarded.

Consider the simplest case of measuring the mobility of an air ion. Suppose that the air ion moves in a uniform electric field of field strength E, and its mobility is inferred from the distance d traversed by the air ion in the direction of the electric field during time t. The mean value of this distance is

$$\bar{d} = kEt = \sqrt{kUt}, \qquad (19.2)$$

where U is the voltage between the mean end point and starting point of air-ion motion. According to the theory of Brownian motion, the random difference $d - \bar{d}$ obeys a normal distribution with mean square deviation

$$\sigma_d = \sqrt{2Dt}, \qquad (19.3)$$

where D is the diffusion coefficient of the air ions. The diffusion coefficient is linked to the mobility via the relationship

$$D = \frac{KTk}{q}, \qquad (19.4)$$

where K is Boltzmann's constant, T is the absolute temperature and q is the charge of the air ion.

The measured value of the mobility is proportional to the distance d, so that the measured mobility also obeys a normal distribution. The relative mean square deviation s_k of the mobility equals the relative mean square deviation s_d of the distance. With the aid of expressions (19.2), (19.3) and (19.4) we obtain

$$s_k = \frac{\sigma_k}{k} = \frac{\sigma_d}{\bar{d}} = \sqrt{\frac{2KT}{qU}}. \qquad (19.5)$$

The function W in this case has the form

$$W(k, k_1) = \frac{1}{\sigma_k \sqrt{2\pi}} \exp\left[-\frac{(k-k_1)^2}{2\sigma_k^2}\right]. \qquad (19.6)$$

From formula (19.5) it follows that the relative error of the mobility measurement depends on the ratio of the mean energy of thermal motion of the air ion to the mean work of displacement of the air ion in the electric field. This fact is of special physical significance, which is fully disclosed only when approaching the problem from the point of view of the kinetic theory. Although there is no direct need for this, we shall briefly follow the simplified derivation of formula (19.5) based on kinetic considerations.

Suppose that the probability distribution of the air-ion velocity at the initial instant is determined only by thermal motion. Consider a short time interval t, in which no collisions of the air ion with molecules occur. Owing to thermal motion the air ion traverses during this time in the direction

of one coordinate axis, a distance whose mean value equals zero and whose mean square deviation is

$$\sigma_d = \sqrt{\frac{KT}{m}}\, t, \tag{19.7}$$

where m is the mass of the air ion. Under the influence of the electric field the air ion acquires the additional velocity qEt/m and traverses the distance

$$d = \frac{qEt^2}{2m} = \sqrt{\frac{qU}{2m}}\, t, \tag{19.8}$$

where U is the voltage drop over the distance d. Calculation of the ratio σ_d/d leads to formula (19.5).

If during the time t one collision occurs, then the latter subdivides the time interval t into two parts, t_1 and t_2. The dispersion of the thermal displacement of the air ions in the interval t_1 is $\sigma_1^2 = \frac{KT}{m} t_1^2$ and in the interval t_2, $\sigma_2^2 = \frac{KT}{m} t_2^2$. The colliding air ion retains on the average a fraction α of the initial momentum. The covariation of the thermal displacements of the air ion in the time intervals t_1, t_2 is therefore $\alpha \frac{KT}{m} t_1 t_2$. The dispersion of the thermal displacement in the interval t is correspondingly expressed by the sum

$$\sigma_d^2 = \frac{KT}{m}(t_1^2 + 2\alpha t_1 t_2 + t_2^2). \tag{19.9}$$

The displacement of the air ion due to the electric field is in the first time interval $d_1 = Eqt_1^2/2m$ and in the second time interval $d_2 = Eq(\alpha t_1 t_2 + t_2^2/2)/m$. The total displacement is then

$$d = \frac{Eq}{2m}(t_1^2 + 2\alpha t_1 t_2 + t_2^2) = \sqrt{\frac{qU}{2m}}\sqrt{t_1^2 + 2\alpha t_1 t_2 + t_2^2}\, t_2^2. \tag{19.10}$$

The ratio σ_d/d is expressed, as previously, by formula (19.5). On the basis of similar arguments we can verify that expression (19.5) holds for an arbitrary number of collisions.

In the aspiration method the time of movement of the air ions is inferred from the drift of the air ion with the air flow. Since diffusion occurs also in the direction of the air flow, this introduces an additional error into the measurement result.

Consider the determination of the mobility in a homogeneous electric field. Here and in subsequent derivations in this section we shall assume that the flow velocity $\vec{u}$ and the field strength $\vec{E}$ of the electric field are perpendicular to one another. If the air ion traverses over a certain time a distance x in the direction of the air flow and a distance y in the direction of the electric field, then its mobility is determined by the relation

$$k = \frac{u}{E}\frac{y}{x}. \tag{19.11}$$

The ratio y/x has no statistical moments, since at $x = 0$ there exists a finite probability density. In order to retain clarity of presentation we shall refrain from full mathematical rigor and introduce certain new concepts. The ratio $\bar{y}/\bar{x}$ will be called the conditional mean of the ratio y/x. The sum $s_y^2 + s_x^2$, which equals the relative variance of the linearized form of the ratio y/x, will be called the conditional relative variance of the ratio y/x. We shall assume that random deviations are considerably less than the mean values of x and y. Then the distribution function of the ratio $\bar{y}/\bar{x}$ practically coincides with the distribution function, whose variance equals the conditional variance of the ratio y/x. For the sake of brevity, we shall omit in the following the word conditional in the definitions "conditional mean" and "conditional variance."

In a homogeneous field $\sigma_x = \sigma_y$ and $s_x = \frac{y}{x} s_y$. The standard deviation σ_u is defined by formula (19.5). Setting $y/x = kE/u$, we obtain

$$s_k = \sqrt{\frac{2KT}{qU}\left(1 + \frac{k^2E^2}{u^2}\right)}. \tag{19.12}$$

The above result may be directly applied to evaluate the effect of diffusion in a counter with a parallel-plate measuring capacitor.

The method of the apparent distribution of mobilities enables us to describe similarly the effect of the diffusion of air ions in the measuring capacitor for the case of an integral as well as a differential counter. In both cases the measurement results depend on the behavior of the critical air ions, which move close to the limiting surface for the mobility k_0.

In a counter with a parallel-plate measuring capacitor, we have for the critical air ions $x = l$ and $y = d$. Accordingly,

$$s_k = \sqrt{\mu \frac{2KT}{qU}}, \tag{19.13}$$

where

$$\mu = 1 + \frac{d^2}{l^2}. \tag{19.14}$$

In the case of a inhomogeneous field matters become more complicated in the coaxial capacitor. We shall make an approximate calculation, whereby we consider the movement of an air ion over short successive segments for which one may use formula (19.12) with sufficient accuracy. The movement of the air ion is determined by the ratio of the air-flow rate and the electric flux $k = \Phi/N$ through the flow surface. If the flow surface consists of successive segments through which the flow rates and electric fluxes are Φ_n and N_n respectively, and the considered air-ions possess different apparent mobilities k_n, in each of those segments we may then write for each segment $k_n = \Phi_n/N_n$. For the entire flow surface the apparent mobility is given by

$$k = \frac{\sum_n \Phi_n}{\sum_n N_n} = \frac{\sum_n N_n k_n}{N}. \tag{19.15}$$

Consequently, the variance of the mobilities is determined by the sum

$$\sigma_k^2 = \frac{\sum_n N_n^2 \sigma_{kn}^2}{N^2}. \tag{19.16}$$

When the critical air ions move through the entire measuring capacitor, $N = 4\pi CU$. For a short segment of the axially symmetric flow surface, we have

$$N_n = 2\pi r_n E_n l_n, \tag{19.17}$$

where l_n is the length of the relevant segment along the capacitor axis. Determining σ_{kn} in accordance with (19.12), and bearing in mind that

$$U_n = \frac{E_n^2 k_n l_n}{u_n}, \tag{19.18}$$

we obtain

$$\sigma_k^2 = \frac{KT}{2q C^2 U^2} \sum_n k_n \left(r_n^2 u_n^2 + r_n^2 E_n^2 k_n^2\right) t_n, \tag{19.19}$$

where $t_n = l_n/u_n$ is the time of passage through the segment l_n.

In the above expression a certain mean mobility may be placed before the summation sign. Thus, assuming the mean mobility is equal to k_0, the expression for s_k can be written in the form of (19.13), where μ is given by

$$\mu = \frac{\pi}{C\Phi}\left(\sum_n r_n^2 u_n^2 t_n + k_0^2 \sum_n r_n^2 E_n^2 t_n\right). \tag{19.20}$$

In this expression it is advisable to switch from summation to integration. A physical interpretation makes this transition seem rather incorrect because of the nonpermissible increase in the variance σ_{kn}^2. The integration should be considered only as a means of effecting an approximate calculation. The final expression of the parameter μ for the axially symmetric measuring capacitor with transverse fields $\vec{u}$ and $\vec{E}$ is

$$\mu = \frac{\pi t_0}{C\Phi}\left[\int_0^1 r^2(\vartheta) u^2(\vartheta)\, d\vartheta + k_0^2 \int_0^1 r^2(\vartheta) E^2(\vartheta)\, d\vartheta\right]. \tag{19.21}$$

The relative time ϑ is defined as

$$\vartheta = \frac{t}{t_0}, \tag{19.22}$$

where the time of passage of the air ion through the capacitor is assumed to be equal to the filling time of the capacitor.

In the absence of radial components of the air flow velocity, we obtain for a cylindrical capacitor

$$r^2(\vartheta) = r_2^2 - \left(r_2^2 - r_1^2\right)\vartheta \tag{19.23}$$

or

$$r^2(\vartheta) = r_1^2 + \left(r_2^2 - r_1^2\right)\vartheta. \tag{19.24}$$

The product rE is constant:

$$rE = \frac{U}{\ln \frac{r_2}{r_1}}. \tag{19.25}$$

In the case of uniform distribution of flow velocities integration is simple and yields

$$\mu = \left(\frac{r_2^2 - r_1^2}{2l^2} + \frac{r_2^2 + r_1^2}{r_2^2 - r_1^2}\right)\ln \frac{r_2}{r_1}. \tag{19.26}$$

For a velocity distribution described by (18.2), integration likewise involves no difficulties, but the resulting formula is awkward and inconvenient. The value of the parameter μ depends only slightly on the profile of the flow velocity, so that formula (19.26) suffices for practical considerations.

The dependence of the parameter μ on the ratios l/r_2 and r_1/r_2 is given in Figure (19.2).

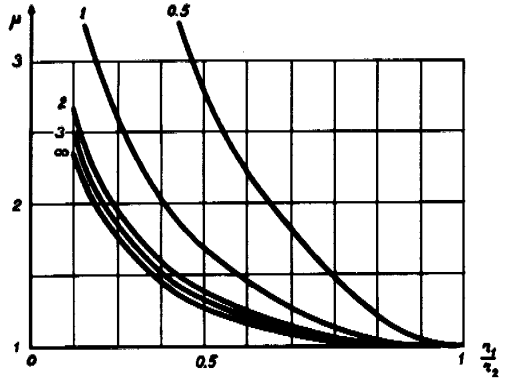

FIGURE 19.2. Dependence of the parameter μ on the dimensions of a cylindrical capacitor. The numbers above the curves denote the values for the ratio l/r_2.

The expression obtained for s_k differs from that given in the work /Tammet, 1962b/, where an unjustified simplification is used. The difference in the results, however, becomes marked only for large values of the ratio r_2/r_1, which are seldom encountered in practice.

Apart from the distortions treated in the present section, diffusion leads to the absorption of air ions. The problem will be dealt with below.

§20. TURBULENT MIXING OF AIR IN A MEASURING CAPACITOR

In the theory of the aspiration method, it is usually assumed that the air flow in the measuring capacitor possesses a laminar character. Sometimes this condition is not satisfied and the air flow in the capacitor is more or less turbulent. The estimation of distortions caused by turbulence is of great interest, since these distortions constitute a decisive factor when choosing the flow rate for the aspirated air. Unfortunately, the effect of turbulence on the measurement results is the most complicated and least studied problem in the theory of the aspiration counter. In early works /Gish, 1933a, 1933b; Wait, 1934; Graziadei, 1935/ only ill-founded, hypothetical propositions on the effect of turbulence on the current generated in the integral counter were made. In these works the absence or presence of turbulence in the measuring capacitor was judged on the basis of the Reynolds number. This, however, leads to doubtful results. Only in the works /Israël, 1931; Wolodkewitsch, Dessauer, 1931b/ was the appearance of turbulence determined by observing a smoke trace in a transparent model of the capacitor. This method of studying the nature of the flow was recently also applied with success /Faucher, 1958; Misaki, 1960; Matulyavichene, 1962/. In the work /Misaki, 1960/ the smoke-trace method was modified to serve as a quantitative measure for determining the flow profile. Israël /Israël, 1931/ showed that turbulence reduces the current generated in the integral counter by approximately 5—10%. This result is disputed in another work /Reimers, 1940/, where, on the basis of experimental data and theoretical considerations, it is maintained that the character of the air flow in the measuring capacitor in no way affects the measurement results. Insufficient accuracy of the experiments and ill-founded theoretical considerations are evidence that this assertion is unreliable.

The most detailed experimental work in the study of turbulent mixing was performed by Yaita and Nitta /Yaita, Nitta, 1955/. The character of the flow was studied with the aid of a thermistor probe. Accordingly, it was found that the effect of turbulence is manifested in the dispersion of the air-ion mobilities. The quantitative results are limited to a few examples in which the characteristics of an integral counter are compared under different operating conditions in a parallel-plate capacitor.

Tammet /Tammet, 1962b/ estimated the intensity and regularity of turbulent mixing from data based on atmospheric turbulence /Richardson, 1926; Teverovskii, 1949/. Ill-founded initial assumptions rendered the results of this work erroneous.

The turbulent mixing of air disperses the air-ion trajectories in the same way as in the case of thermal diffusion. According to (19.1) this leads to a smoothing of the spectrum $\varrho(k)$. In the following calculations we shall neglect thermal diffusion.

The turbulent flow field may be resolved into the mean field $\vec{u}_0$ and the field of turbulent fluctuations $\vec{u}_t$. The field $\vec{u}_0$ is time-independent and has properties which should be characteristic of the flow field in the measuring capacitor of the counter. Deviations from ideal operating conditions of the counter are caused by the additional field $\vec{u}_t$. The mean value of $\vec{u}_t$ is equal to zero by definition, so that turbulent pulsations do not affect the mean

distance traversed by the air ion over a given period. Consequently, in the first approximation turbulent mixing will not distort the mean values of the measured mobilities. This is confirmed by experimental results described in the following section.

As in the preceding paragraph we shall assume that the fields $\vec{E}$ and $\vec{u}_0$ are perpendicular to one another. Consider the movement of an air ion during the short time interval t_n. The time t_n should be sufficiently small, so that the inhomogeneity of the electric field and the mean air velocity along the trajectory of the air ion can be neglected. The time t_n should also be small compared to the Lagrangian microscale of turbulence. The mean displacement of the air ions in the direction during the time t_n is $\bar{x}_n = u_0 t_n$; the variance of this displacement is $\sigma_x^2 = \overline{u_{tx}^2} t_n^2$. Correspondingly, the displacement along the electric field is $\bar{y}_n = kEt_n$, and the variance is $\sigma_y^2 = \overline{u_{ty}^2}\, t_n^2$. The apparent mobility of an air ion is proportional to the ratio y_n/x_n. Remembering that the ratio $\overline{u_t^2}/u_0^2$ usually does not exceed 100, the relative variance of the apparent mobility can be calculated as follows:

$$s_k^2 = s_x^2 + s_y^2 - 2R_{x,y}s_x s_y \tag{20.1}$$

where $R_{x,y}$ is the correlation coefficient between u_{tx} and u_{ty}. Since the coordinate axes of the correlation are at right angles, $R_{x,y}$ is small remote from the plates. When moving from one plate of the measuring capacitor to the other, $R_{x,y}$ changes sign and, when averaged, is practically equal to zero. Suppose $R_{x,y} = 0$. Then

$$s_k = \varepsilon \sqrt{1 + \frac{u_0^2}{k^2E^2}}. \tag{20.2}$$

ε is a certain mean intensity of turbulence. Assuming that $\overline{u_{tx}^2} = \overline{u_{ty}^2} = \overline{u_{txy}^2}$, ε is expressed by

$$\varepsilon = \frac{\sqrt{\overline{u_{txy}^2}}}{u_0}. \tag{20.3}$$

If the air ion has different apparent mobilities k_n in the successive time intervals t_n, then the apparent mobility determined from the movement of air ions over a longer time interval can be calculated by formula (19.15). When determining the dispersion of the apparent mobility, we must allow for the characteristics of the turbulent diffusion /Batchelor, 1953; Frenkiel, 1953; Pai, 1957; Monin, Yaglom, 1965, 1967/. In the case of the thermal diffusion, the deviations of the apparent mobility from the mean $k_n - \bar{k}$ in successive time intervals could be considered as independent, but in the case of the turbulent diffusion, the situation is more involved. The deviations $k_n - \bar{k}$ and $k_m - \bar{k}$ are correlated with one another. Denoting the correlation coefficient between the above deviations by $R_{n,m}$, we obtain the following expression for the variance:

$$\sigma_k^2 = \sum_n \sum_m R_{n.}\ \frac{N_n N_m}{N^2}\ \sigma_{kn}\sigma_{km}. \tag{20.4}$$

We now utilize formula (19.17), and, after replacing t_n by dt, we switch from summation to integration:

$$\sigma_k^2 = \frac{4\pi^2}{N^2}\int_0^{t_0}\int_0^{t_0} R(t_1,t_2)r(t_1)E(t_1)u_0(t_1)\sigma_k(t_1)\times$$
$$\times r(t_2)E(t_2)u_0(t_2)\sigma_k(t_2)\,dt_1dt_2. \qquad (20.5)$$

$R(t_1, t_2)$ is the Lagrangian correlation function of the apparent mobility along the trajectory of the air ion.

To simplify the notation, we change over to the relative time scale and introduce the dimensionless quantity

$$w(\vartheta) = \frac{2\pi r(\vartheta)E(\vartheta)u_0(\vartheta)t_0}{N}. \qquad (20.6)$$

The relative variance of the apparent mobility of the critical air ion in the measuring capacitor is now given by

$$s_k^2 = \int_0^1\int_0^1 R(\vartheta_1,\vartheta_2)w(\vartheta_1)w(\vartheta_2)s_k(\vartheta_1)s_k(\vartheta_2)\,d\vartheta_1d\vartheta_2. \qquad (20.7)$$

Let us now carry out the calculation for a cylindrical measuring capacitor, assuming that the field $\vec{u_0}$ is homogeneous. It can be readily shown that in this case $w(\vartheta) = 1$. The expression for $R(\vartheta_1, \vartheta_2)$ is unknown, which compels us to confine ourselves to an approximate solution. We place the correlation function $R(\vartheta_1, \vartheta_2)$ before the integral sign, using the mean-value theorem. The corresponding mean value will be denoted by $\bar{R}$ and will be called the relative effective scale of turbulence in the measuring capacitor. Thus, we place before the integral sign the effective turbulent intensity $\bar{\varepsilon}$, which is the corresponding mean value of the quantity $\varepsilon(\vartheta)$. As a result, we obtain

$$s_k = \mu_t\bar{\varepsilon}\sqrt{\bar{R}}, \qquad (20.8)$$

where

$$\mu_t = \int_0^1 \sqrt{1+\frac{u_0^2(\vartheta)}{k_0^2E^2(\vartheta)}}\,d\vartheta. \qquad (20.9)$$

Integration yields for the cylindrical measuring capacitor

$$\mu_t = \frac{r_2^2-r_1^2}{6l^2}\left\{\left[1+\frac{4l^2r_2^2}{(r_2^2-r_1^2)^2}\right]^{3/2} - \left[1+\frac{4l^2r_1^2}{(r_2^2-r_1^2)^2}\right]^{3/2}\right\} \qquad (20.10)$$

Figure 20.1 shows curves plotted in accordance with the above formula.

A similar calculation for the parallel-plate capacitor leads to the same formula (20.8). However, the parameter μ_t is now expressed by

$$\mu_t = \sqrt{1+\frac{l^2}{d^2}}. \qquad (20.11)$$

In (20.8) the quantities $\bar{R}$ and ε remain undefined. Therefore, the above calculations do not yield any direct practical results, but merely serve the purpose of creating a qualitative picture of the effect of the turbulent mixing in the measuring capacitor. Formula (20.8) may be used for a quantitative estimation only in the absence of more accurate data. In the case of a completely turbulent flow in the cylinders ε is of the order of about 1/20 /Hinze, 1959/, and the relative scale $\bar{R}$ may be estimated from the ratio of $r_2 - r_1$ and the length of the trajectory of the critical air ions.

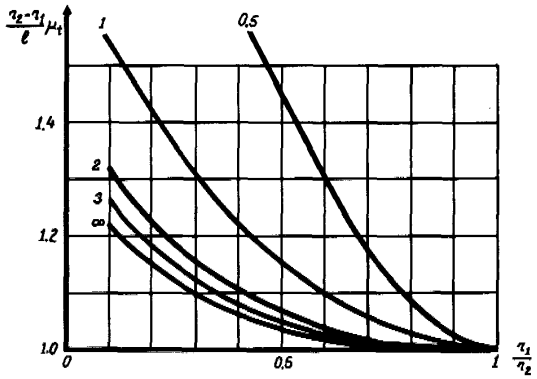

FIGURE 20.1. Dependence of the parameter μ_t on the dimensions of the cylindrical capacitor. Numbers above the curves correspond to values of the ratio l/r_2.

In principle, the quantity $\bar{\varepsilon}\sqrt{\bar{R}}$ may be estimated more accurately when using the well-known semiempirical theories of turbulence and the available data obtained in experimental investigations of turbulent flow in tubes and channels /Pai, 1957; Hinze, 1959; Gkhosh, 1968/. However, this leads to rather involved calculations and the accuracy obtained is still doubtful. In addition to this, the initial data necessary for such calculations are known only in a limited number of cases. We are thus compelled to prefer another approach, for example, the direct experimental investigation of the effect of turbulent mixing of air in the measuring capacitor.

Finally, we note that turbulent mixing as well as diffusion of air ions has practical significance, particularly in the study of the air-ion spectrum. The effect of turbulence on the current generated in the integral counter is not very strong and causes only a slight reduction in the latter. The error reaches a maximum if the air contains air ions of mobility $k = k_0$ only. The relative error in this case is determined approximately by the formula

$$\delta_I = \frac{1}{2} + \frac{s_k}{\sqrt{2\pi}}\left[1-\exp\left(-\frac{1}{2s_k^2}\right)\right] - \frac{1}{2}\operatorname{erf}\left(\frac{1}{\sqrt{2}\,s_k}\right). \qquad (20.12)$$

For $s_k < 30\%$ a sufficient accuracy in ensured by the simplified formula

$$\delta_I \approx 0.4s_k. \qquad (20.13)$$

Of practical significance is also the effect of turbulent mixing on the adsorption of air ions /Siksna, Metnieks, 1953; Zachek, 1964b/.

§21. RESULTS OF THE EXPERIMENTAL INVESTIGATION OF THE EFFECT OF TURBULENCE

The main purpose of the experiments described below is to study the character of the dependence of the mobility dispersion on turbulence, on the parameters and operating conditions of the measuring capacitor, as well as on the air conditions at the counter inlet. Together with this, the task of the compiling data for a rough quantitative estimate of the effect of turbulent mixing on the measurement results was kept in mind.

The following requirements were imposed on the experimental counter:

1. The counter should have a high resolving power, so that the smoothing of the spectrum by turbulent mixing can be detected and quantitatively measured. The smoothing of the spectrum should be prevented because of the adsorption of air ions.
2. So as not to complicate the aerodynamical properties of the counter inlet, methods requiring the separation of the air flow should not be employed.
3. The design of the counter should ensure the possibility of using interchangeable inner plates of different lengths and radii, while maintaining the radius of the outer plate.

These requirements compel us to select the principle of the first-order differential counter with a divided capacitor and an outer collector plate. The arrangement of the measuring capacitor is schematically shown in Figure 21.1. The inner plate may be optionally displaced toward the inlet opening or in the opposite direction, allowing us to regulate the effective length of the measuring capacitor. The effective length was determined by a calculation method which will be described in §33.

Another suitable method for the experimental investigation of turbulent mixing in the measuring capacitor is the use of an integral counter with an oppositely charged precondenser (Figure 9.1). Here, operating conditions can be used, whereby the current generated in the main capacitor occurs only in the case of dispersion of the apparent mobilities of the air ions. In the present book, the last method was not used because it was judged to be less suitable under the condition that there was no preliminary information on the character of turbulent mixing in counters.

The circuit diagram and the air path of the counter used here are shown in Figure 21.2. The voltage was applied to the inner plate by a P82 potentiometer from the VS-22 rectifier, which ensured a highly stable voltage up to 4000 volts. The voltage of the inner plate was measured with the aid of an M502 voltmeter (accuracy ± 0.1 V). The current through the collector plate was measured by the method described in §15. The air-flow rate was measured with the aid of a gas counter of the type GKF or RS-40, which were previously calibrated with the aid of a calibrated 0.6-m^3 container filled with water. Sudden changes in the air flow due to the gas counter were smoothed with the aid of a drum having a rubber cover and an effective volume of about 1 m^3. The correction for the pressure difference, which became marked at high flow rates, was allowed for. To calculate the correction the temperature difference in the system was measured.

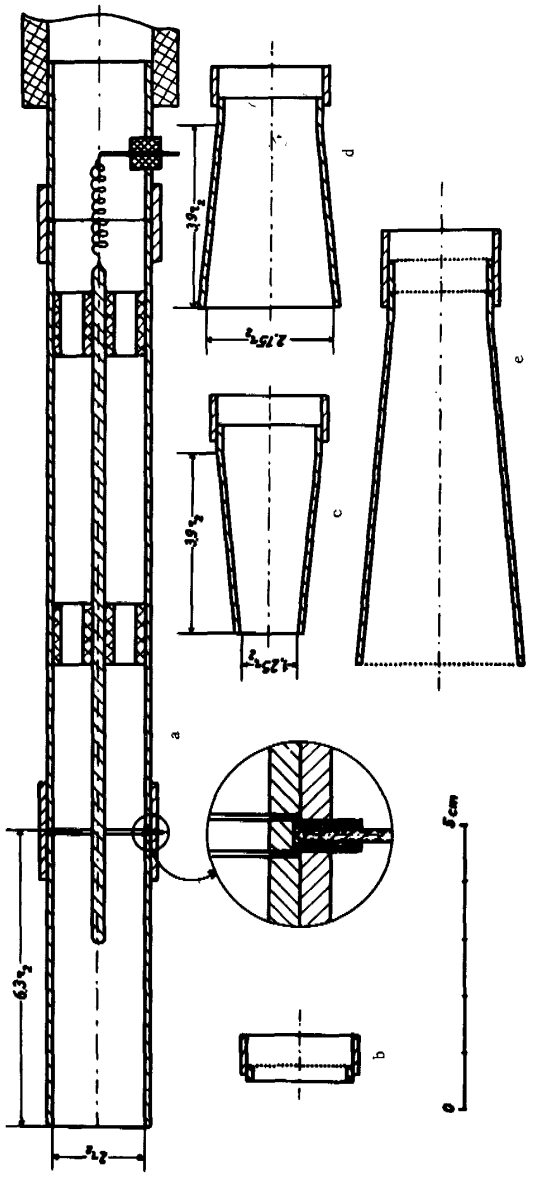

FIGURE 21.1. a—measuring capacitor; b—nozzle with grid ($k = 0{,}055\ r_1$, $r_0 = 0{,}0085\ r_2$); c—diffuser nozzle; d—nozzle; e—laminarizing nozzle with three grids.

A highly stable source of air ions was necessary in order to perform the experiment. The ion generator must be sufficiently powerful, so that the ionization of air drawn into the measuring capacitor does not depend appreciably on the flow rate. The age of the generated air ions at the inlet of the counter should be not less than half a second, so that the spectrum $\varrho(k)$ will have enough time to stabilize and will not change while the air is passing through the measuring capacitor. In addition to this, it is necessary to create a turbulent field at the inlet of the counters which corresponds to conditions encountered in the atmospheric layer near the ground. The turbulent field must be sufficiently stable. Keeping the above-mentioned requirements in mind, a special ion generator was designed and built (see Figure 21.3). The air ions are generated in equal quantities for both polarities. The maximum obtainable polar charge density was 170,000 e.s.u./cm^3. The ionizing power is regulated by placing aluminum disks under a radioactive preparation. The mean linear air velocity in the ion generator was 2.15 m/sec, and the flow rate 0.245 m^3/sec. The turbulent intensity can be reduced by letting the air flow through a grid placed at the outlet of the ion generator. The turbulent intensity was not measured, since a suitable instrument was not available.

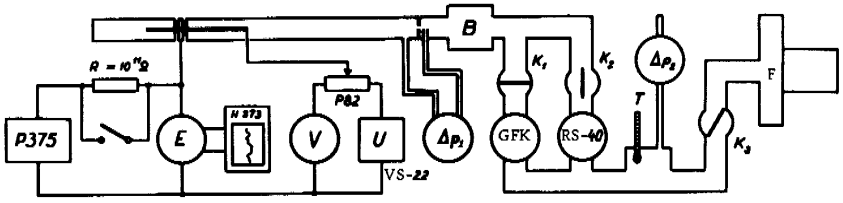

FIGURE 21.2. Circuit diagram of the counter. E—dynamic electrometer; Δp_1—differential manometer of the flow meter; B—shock drum; K_1 and K_2—two-way stopcocks of the flowmeters; K_3—control stopcock; F—fan operating at $\Delta p = 600\,\text{kg/m}^2$.

The air-ion spectrum was determined for Re = 1200, $l/r_2 = 2.5$ and $r_2/r_1 = 8.4$. The counter was provided with a laminarizing unit consisting of a nozzle and grids. Preliminary experiments showed that such conditions ensured a resolving power close to the best possible resolving power which can be obtained upon varying the operating conditions of the described counter. The results of the spectrum are given in Figure 15.2. Further measurements were carried out with positive air ions, the spectral distribution of which is quite close to a normal Gaussian distribution. This specifically applies to the left-hand part of the spectral distribution, which cannot be distinguished from the normal distribution curve with a relative variance $s_k^2 = 0.016$. Preliminary experiments also showed that the character of the spectral distribution remains similar to a normal distribution even when turbulence occurs in the counter.

These preliminary results greatly simplified the experimental layout for further experiments. To find the dispersion it is not necessary to determine the spectrum in detail. Instead, the method described below was used.

We shall determine the voltage U^*, which for laminar air flow satisfies the condition

$$I(U^*) = I(U^*/2). \tag{21.1}$$

Assuming a normal distribution of mobilities with a relative variance of $s_k^2 = 0.016$, we obtain

$$U^* = 0{,}984\,\frac{\Phi}{4\pi\bar{C}\bar{k}}, \tag{21.2}$$

where $\bar{C} = C_1 + C_2/2$ is the mean effective capacitance and $\bar{k}$ is the mean mobility. Since the accuracy in determining the mean effective capacitance is relatively low, the value of U^* was accurately adjusted for each electrode geometry. To do this, four measurements were performed at the respective voltages U_a, U_b, $U_a/2$, $U_b/2$, where U_a and U_b were chosen close to U^*. The exact value of U^* was determined from the measurement results by means of graphical solution of equation (21.1). For a change in the flow rate, while maintaining the electrode geometry unaltered, U^* was calculated from the relationship $U_2^*/\Phi_2 = U_1^*/\Phi_1$.

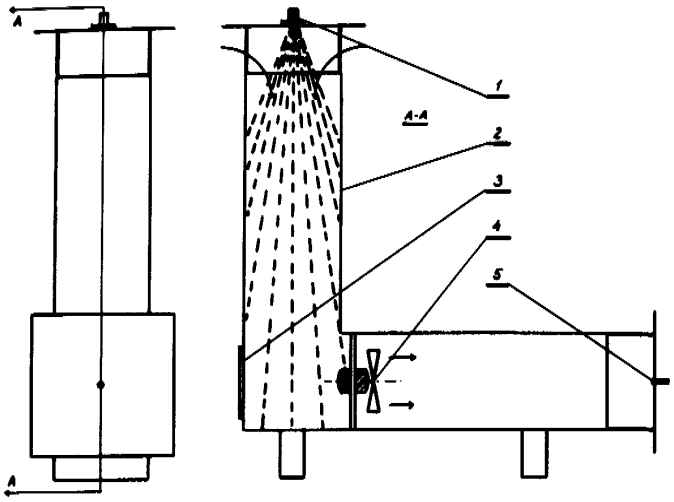

FIGURE 21.3. Ion generator. 1—preparation Sr^{90} (10 mCi); 2—air channel; 3—door; 4—fan; 5—measuring capacitor of the counter.

To determine the variance the current was measured at voltages $U_1 = 0.8\,U^*$ and $U_2 = 1.3\,U^*$, respectively. From these measurements the auxiliary value

$$Z = \frac{I(U_2)}{I(U_1)}, \tag{21.3}$$

was calculated, which is related to the relative variance of the spectrum. Assuming a normal distribution, we obtain

$$Z = 1.625 \frac{\operatorname{erf}\frac{1}{\sqrt{2}\,s_k} - \operatorname{erf}\frac{0.2185}{\sqrt{2}\,s_k} - \sqrt{\frac{2}{\pi}}\,s_k\left[\exp\left(-\frac{0.0477}{2s_k^2}\right) - \exp\left(-\frac{1}{2s_k^2}\right)\right]}{\operatorname{erf}\frac{1}{\sqrt{2}\,s_k} - \operatorname{erf}\frac{0.2700}{\sqrt{2}\,s_k} - \sqrt{\frac{2}{\pi}}\,s_k\left[\exp\left(-\frac{0.0729}{2s_k^2}\right) - \exp\left(-\frac{1}{2s_k^2}\right)\right]}. \qquad (21.4)$$

The dependence $s_k^2 = s_k^2(Z)$, plotted in accordance with (21.4), is shown in Figure 21.4. The parameter Z appears to be quite a sensitive indicator of small changes in the variance of the spectrum.

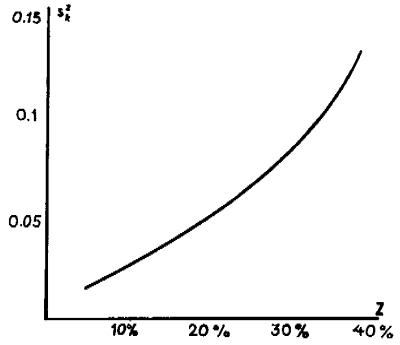

FIGURE 21.4. Graph of function $s_k^2(Z)$

Note that the auxiliary value Z depends essentially on the behavior of air ions, the mobility of which is less than the mean mobility. As mentioned above, the assumption of a normal distribution of mobilities is valid in the range in question. This is sufficient reason to assume that the accuracy of the described method is satisfactory. Considerable deviations from a normal distribution may arise only in the case of particularly large variances. Therefore, the standard deviations, obtained with the aid of the described method and which exceed 20—30%, are inaccurate and have rather the character of some conditional parameter.

As an example, Figure 21.5 shows the characteristics of a counter for relative variances of 0.016 and 0.100. The points U^*, U_1, U_2 and the method for the graphical solution of equation (21.1), can be seen in the figure.

When smoothing the spectrum successively with the aid of certain smoothing functions, the relative variances of the spectrum and the smoothing functions are cumulative, so that the relative variance of the apparent spectrum becomes

$$s_k^2 = s_{k0}^2 + s_{k\Delta}^2 + s_{kd}^2 + s_{kt}^2, \qquad (21.5)$$

where $s_{k\Delta}^2$ is due to the finite length of the collector plate; s_{kd}^2 is due to the thermal diffusion of air ions; s_{kt}^2 is due to turbulent mixing; and s_{k0}^2 is due to the actual spectral distribution and to unmentioned smoothing factors which play a secondary role.

The variance $s_{k\Delta}^2$ is determined from formulas (7.6) and (7.11). After carrying out the relevant calculations, we obtain

$$s_{k\Delta}^2 = \frac{1}{12}\left(\frac{\Delta l}{l}\right)^2. \qquad (21.6)$$

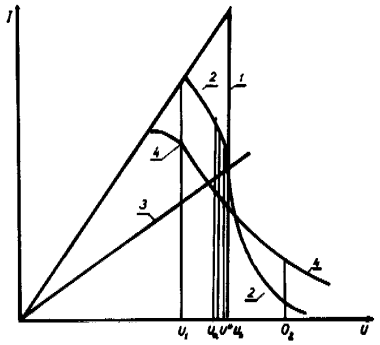

FIGURE 21.5. Counter characteristics: 1—for $s_k^2 = 0$; 2—for $s_k^2 = 0.016$; 3— $I(U/2)$ for $s_k^2 = 0.016$; 4— $I(U)$ for $s_k^2 = 0.1$.

The variance s_{kd}^2 is calculated in accordance with formulas (19.13) and (19.26). The variance s_{k0}^2 must be determined experimentally. To do this, operating conditions must be attained for which $s_{kt}^2 = 0$. The laminarizing nozzle shown in Figure 21.1 helped to prevent turbulence. The electrode geometry was specified by the ratios $l'/r_2 = 3.8$, $l/r = 2.5$, and $r_3/r_1 = 8.4$. The dependence $s_k^2 = s_k^2$ (Re) was determined with the aid of an earlier described method.

The Reynolds number Re was calculated from

$$\mathrm{Re} = \frac{\Phi}{\pi\nu r_2}. \qquad (21.7)$$

The results are listed in Table 21.1.

These results enable us to assume that at Re $\leqslant$ 1400 there is no turbulent mixing of air in the counter. To verify this, several experiments at Re = 1400 were carried out. First, the ion generator was provided with a grid which reduced the level of internal turbulent fluctuations. In the experiment without a laminarizing nozzle, the value of s_k^2 decreased from 0.2 to 0.09. With the laminarizing nozzle, we obtained $s_k^2 = 0.0163$ in both cases. Hence, it follows that external turbulence does not penetrate through the laminarizing nozzle. Secondly, a tube of length $29\,r_2$ was mounted between the measuring capacitor and the laminarizing nozzle.

This also did not alter the variance s_k^2. Consequently, no turbulence occurs inside the capacitor.

The described experiments at the same time constitute an experimental verification of the theory of the diffusion dispersion of mobilities. The results listed in the first three columns of Table 21.1 agree well with the theoretical conclusions (§19), on the basis of which the variances s_{kd}^2 were calculated.

TABLE 21.1

Re	570	1115	1400	1920	2980	5030
s_k^2	0.0183	0.0165	0.0163	0.0189	0.0207	0.0211
$s_{k\Delta}^2$	0.0002	0.0002	0.0002	0.0002	0.0002	0.0002
s_{kd}^2	0.0039	0.0019	0.0016	0.0012	0.0008	0.0004
$s_{k0}^2 + s_{kt}^2$	0.0142	0.0144	0.0145	0.0177	0.0199	0.0205

A series of basic measurements was carried out over the shortest possible time interval in order to prevent marked variations in the external conditions. The experiments were performed in a basement which rendered the test easier. Over a period of six days, which was the time necessary for the measurements, the air temperature varied from 21° to 24°, the relative humidity from 42% to 52% and the atmospheric pressure from 756 mm to 766mm Hg. Each day, prior to carrying out the measurements, the exact value of U^* and the variance s_{k0}^2 were determined.

The values of s_{k0}^2 were 0.0141, 0.0145, 0.0144, 0.0144, 0.0149 and 0.0144, respectively. The relative standard deviation of the parameter s_{k0} from the mean value was 0.9%. This value characterizes the stability of the relative spectral distribution of air ions for the described conditions.

The length l' of the frontal section was varied by mounting tubular sections between the measuring capacitor and entrance nozzle. The results are graphically shown in Figure 21.6.

From the curves in Figure 21.6, it immediately follows that s_{kt} depends strongly on the turbulence of the air entering the counter. For intermediate lengths of the frontal sections the external turbulence and the entrance conditions of the air play a decisive role in the turbulent smoothing of the spectrum.

Another interesting result is that in a counter without a laminarizing nozzle and without tubular sections (curve 1, Figure 21.6) s_{kt} decreases with increasing air flow rate, even at high values of Re. This emphasizes the incompatibility of the traditional viewpoint on the problem of preventing turbulence in counters. The observed "reciprocal" dependence of s_{kt} on Re is fully explicable. Small-scale turbulent pulsations penetrate with the aspirated air into the measuring capacitor. The turbulent intensity at the beginning of the measuring capacitor is determined by the ratio of the mean

square value of the fluctuation and the mean airflow velocity. Consequently, the turbulent intensity decreases with increasing flow velocity.

In the described experiments the intensity of the turbulence penetrating from the outside considerably exceeds the turbulent intensity of the steady flow in the tube. The initial turbulence gradually diminishes as air flows through the measuring capacitor. In the long tubular attachment the initial turbulence decreases considerably and the variance s_{kt}^2 depends only slightly on the conditions under which the air enters into the counter. These conclusions are borne out by the behavior of curves 9—12, Figure 21.6.

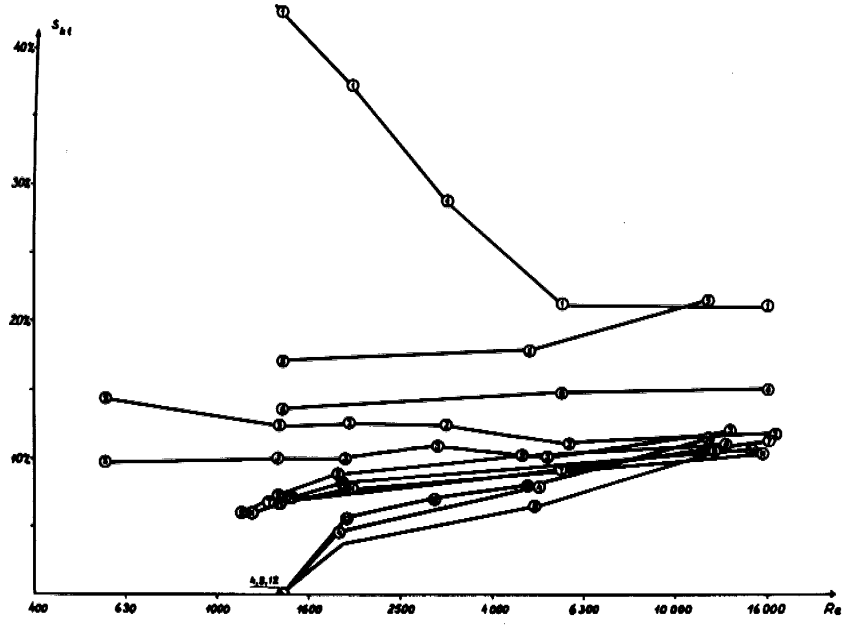

FIGURE 21.6. Turbulent dispersion of mobilities. The type of nozzle (Figure 21.1) and the value of the ratio l'/r_2 (in parentheses) are given for the respective curves:

1—without nozzle (3.8); 2—d (3.8); 3—b (3.8); 4—e (3.8); 5—c (14.3); 6—without nozzle (14.3); 7—d (14.3); 8—e (14.3); 9—c (33); 10—without nozzle (33); 11—d (33); 12—e (33).

The effect of the conicity of the entrance section of the measuring capacitor appears to be extremely strong. In the widening flow (nozzle, Figure 21.2, c) particularly vigorous turbulence is generated, which in the above experiment exceeds even the level of the external turbulence. In the case of a short cylindrical entrance section the parameter Z reached values up to 65%, which does not permit calculating the variance with the aid of the applied method. Therefore, the corresponding data do not appear in Figure 21.6. On the contrary, the convergent channel section strongly

suppresses the external turbulence. This is in good agreement with the well-known results of a study on the stability of converging and diverging currents /Loytsyanskii, 1959/.

An effective means for the suppression of turbulence in the measuring capacitor is the use of a grid attached to the inlet (curves 1 and 3, Figure 21.6).

The dependence of s_{kt} on the effective length of the measuring capacitor was studied for the conditions Re = 1400, $r_2/r_1 = 8.4$; $(l'+l)/r_2 = 17$. The air was drawn into the counter via a converging channel. The measuring results are shown in Table 21.2.

TABLE 21.2

l/r_2	1	2.5	6
s_{kt}^2	0.0037	0.0057	0.026
$\overline{\varepsilon}\sqrt{\overline{R}}$	0.035	0.022	0.019

The values of the parameter $\overline{\varepsilon}\sqrt{\overline{R}}$ are calculated from experimental data according to formula (20.8). The decrease of $\overline{\varepsilon}\sqrt{\overline{R}}$ with increasing length of the measuring capacitor is explained by the decrease of $\sqrt{\overline{R}}$. The mean turbulent intensity $\overline{\varepsilon}$ increases slightly with the length l because of the decrease in the length l' of the frontal section. For comparison, we note that for an inner plate with $l/r_2 = 2.5$ under the same conditions the following values were obtained: for $l'/r_2 = 3.8$, $\overline{\varepsilon}\sqrt{\overline{R}} = 3.6\%$; for $l'/r_2 = 14.5$, $\overline{\varepsilon}\sqrt{\overline{R}} = 2.2\%$; for $l'/r_2 = 33$, $\overline{\varepsilon}\sqrt{\overline{R}} = 1.8\%$.

The measurement results in the case of long and intermediate frontal sections, and large Reynolds numbers agree well with a rough determination of the parameter $\overline{\varepsilon}\sqrt{\overline{R}}$ according to the method described at the end of the preceding section.

A number of experiments was performed to clarify the effect of the geometry of the end of the inner plate on the turbulent mixing. The results of these experiments are mostly of a qualitative nature and we shall therefore refrain from stating any values. In the case of a thin plate ($r_2/r_1 = 8.4$), no considerable influence of the geometry of the end of the inner plate was observed. For the ratio $r_2/r_1 = 2.7$ turbulence started at a lower flow rate and the variance s_{kt} of the mobility due to turbulence was larger when the end of the inner plate had the form of a transversely truncated hollow cylinder. No differences were observed between the results obtained with an inner plate having a flat, semispherical and semiellipsoidal end, respectively.

For $r_2/r_1 = 1.17$ a considerable dependence of turbulent mixing on the geometry of the end of the inner plate was observed. The intensity of turbulent mixing increases in the following order of plate-end geometries: semiellipsoidal, semispherical and flat.

The investigation of the dependence of s_{kt} on the ratio r_2/r_1, with the aid of the above experimental arrangement, proved successful, since upon changing the radius of the inner plate the transition conditions of air from the section with a circular cross section to the section with an annular cross section are not preserved, which essentially affects the character of the flow. This introduces an uncertainty into the measurement results which does not allow us to make any concrete statements.

§22. LONG MEASURING CAPACITOR WITH A TURBULENT AIR FLOW

In the preceding sections the mobility dispersion due to turbulence is assumed to be relatively small. Without this assumption the problem becomes considerably more complex. There exists, however, a very simple solution of the problem in the limiting case of very strong turbulent mixing in a long measuring capacitor. This solution is of practical importance since it determines the upper limit of distortions which can be caused by turbulence.

In the limiting case of a long capacitor with vigorous air mixing, the function $\varrho(k)$ between the plates can be considered to be independent of the radial coordinate of the point under consideration. $\varrho(k)$ will be a function of the distance x of this point from the beginning of the measuring capacitor.

The equation describing the characteristics of the integral counter under these conditions was derived already in the work /Becker, 1910/. Below we shall consider this equation in a somewhat altered form. Let us first suppose that the air contains air ions of mobility k only. For a short section of the cylindrical measuring capacitor we can write

$$dI = 4\pi U \lambda_{\pm}\, dC = \Phi \frac{k}{k_0} \varrho(x) \frac{dx}{l}, \tag{22.1}$$

where k_0 is given by (4.3).

$\varrho(x)$ decreases in this section by the value $dI(x)/\Phi$. Consequently, the equation for $\varrho(x)$ has the form

$$\frac{d\varrho(x)}{dx} = -\frac{k\varrho(x)}{k_0 l} \tag{22.2}$$

Integrating this equation for the condition $\varrho(0) = \varrho_0$, we obtain

$$\varrho(x) = \varrho_0 \exp\left(-\frac{kx}{k_0 l}\right). \tag{22.3}$$

The current through the collector plate of the counter is computed by the integral

$$I = \frac{\Phi k}{k_0 l} \int_0^l \varrho(x)\, dx. \tag{22.4}$$

The function G is defined as the ratio I/Q_0. Integrating, we obtain

$$G = \Phi\left[1 - \exp\left(-\frac{k}{k_0}\right)\right]. \tag{22.5}$$

In Figure 21.1 the curve of the function G for the above case is compared with the curve for an ideal counter.

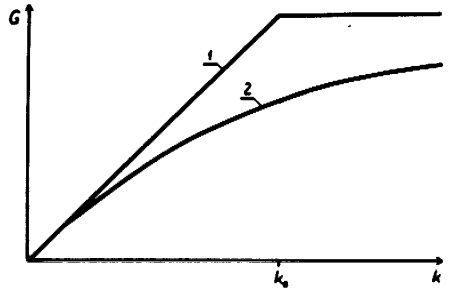

FIGURE 22.1. Function G of an integral counter:

1—laminar flow; 2—complete mixing.

The obtained form of the function G is inconvenient for solving equation (3.3). The study of the spectrum of air ions under these conditions is senseless and we shall therefore consider only the errors arising in the calculation of the polar conductivities and the polar charge densities, using the well-known formulas derived under the assumption of laminar flow. The greatest distortions in the conductivity will arise when the mobility of all the air ions is equal to the maximum mobility k_{max} of air ions actually encountered. To ensure that the relative error will not exceed the value δ, a sufficiently large limiting mobility should be chosen. The minimum permissible values k_0, calculated according to the divergence between the G-functions in (22.5) and (4.4), respectively, are listed in Table 22.1. When measuring the polar charge density, one should start with the minimum value k_{min} of the encountered mobility and restrict k_0 to a sufficiently small value. The permissible limit of the value k_0 for different δ-values is also shown in Table 22.1.

As can be seen from the results, turbulent mixing constitutes a negative influence when measuring polar conductivities.

Allowance for the true form of the curve $q(k)$ ensures less stringent restrictions. It is easy to show that for the condition

$$k_0 \geqslant k_{max} \tag{22.6}$$

we obtain

$$\delta_\lambda = \frac{\int_0^\infty \frac{k}{2k_0}\left(1 - \frac{1}{3}\frac{k}{k_0} + \frac{1}{12}\frac{k^2}{k_0^2} - \frac{1}{60}\frac{k^3}{k_0^3} + \ldots\right)\lambda(k)\,dk}{\int_0^\infty \lambda(k)\,dk}. \tag{22.7}$$

Correspondingly, for the condition

$$k_0 \leqslant k_{min} \tag{22.8}$$

we obtain

$$\delta_q = \frac{\int_0^\infty \exp\left(-\frac{k}{k_0}\right) q(k)\,dk}{\int_0^\infty q(k)\,dk}. \tag{22.9}$$

TABLE 22.1

Permissible error	Permissible k_0	
	Measurement of $\lambda_\pm$	Measurement of q_*
1%	$k_0 \geqslant 50\ k_{max}$	$k_0 \leqslant k_{min}/4.6$
2%	$k_0 \geqslant 24.6\ k_{max}$	$k_0 \leqslant k_{min}/3.9$
5%	$k_0 \geqslant 9.7\ k_{max}$	$k_0 \leqslant k_{min}/3$
10%	$k_0 \geqslant 4.7\ k_{max}$	$k_0 \leqslant k_{min}/2.3$
20%	$k_0 \geqslant 2.2\ k_{max}$	$k_0 \leqslant k_{min}/1.6$

However, complete mixing, as assumed in the above calculations, is never attained in practice. The experimental verification of the manner in which the air ions settle in a long capacitor with a turbulent air flow was carried out with the setup described in §21. The parameters of the counter were: $r_2/r_1 = 2.7$, $l/r_2 = 17$, $l'/r_2 = 18$, $\mathrm{Re} = 15{,}500$. The air was drawn into the measuring capacitor through a convergent channel.

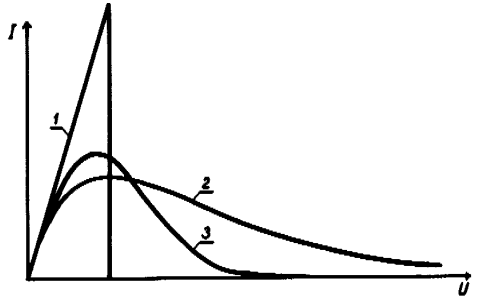

FIGURE 22.2. Characteristics of a differential counter:

1—laminar flow; 2—complete mixing; 3—according to experimental results.

In the case of complete air mixing the function G of the first-order differential counter with a divided capacitor has the form

$$G = \Phi \frac{C_2}{C_1} \frac{k}{k_0} \exp\left(-\frac{k}{k_0}\right). \qquad (22.10)$$

The above formula holds if the ratio C_2/C_1 is small. In the experiment described, $C_2/C_1 = 0.007$, which justifies the approximation employed.

The experimental results are given in Figure 22.2. For comparison, the figure shows the characteristics of a counter for laminar flow conditions and those of a counter for conditions of complete mixing (formula (22.10)).

§23. THE ASYMMETRY OF THE MEASURING CAPACITOR AND THE EFFECT OF GRAVITATION ON AIR IONS

The intricacy of a cylindrical measuring capacitor depends on how accurately the inner plate is centered. To determine the required accuracy, we must know the dependence of the arising errors on the eccentricity of the cylindrical plates.

Consider an asymmetrical measuring capacitor of an integral counter. For small voltages the limiting surface intersects the inlet cross section, and the function G equals $4\pi CUk$, i.e., it does not differ from the function G of a symmetrical counter. An increase in the voltage causes the limiting surface to intersect the second plate. However, because of the asymmetry, the limiting surface will not enclose the entire flow. Here, the function G is then less than $4\pi CUk$, but also less than Φ. Only a further increase in the voltage causes the limiting surface to enclose the entire air flow, and the function G attains the value of Φ. An approximation of the function for an asymmetrical measuring capacitor is shown in Figure 23.1.

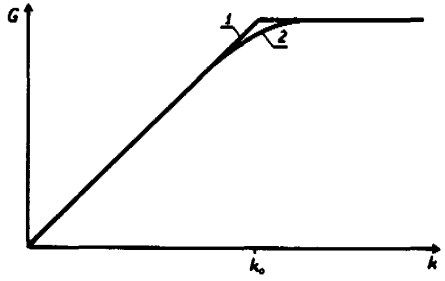

FIGURE 23.1. Function G of an integral counter:

1—for a symmetrical capacitor; 2—for an asymmetrical capacitor.

The effect of the asymmetry of the measuring capacitor on the measurement results can be described also by the method of the apparent spectral

distribution used in §19 and §20. In equation (3.3) the undistorted form of the function G is preserved and the distortions are described as the dispersion of the apparent mobilities. It can be readily verified that the interval of dispersion of the apparent mobilities coincides with the interval of mobilities in which the function G is distorted.

We shall carry out the calculation for a cylindrical capacitor in which the axes of the plates are parallel but displaced by a distance Δr. For simplicity, we make two approximations: 1) we assume that the profile of the air flow is homogeneous, 2) we also assume that $\Delta r \ll r_2 - r_1$, and then carry out the corresponding calculations in the first approximation.

The transverse cross section of the capacitor with an off-center inner electrode is shown in Figure 23.2. The electric field in the capacitor coincides with the field of two charged filaments at distances f_1 and f_2, respectively, from the axis of the outer plate /Landau, Lifschitz, 1957/.

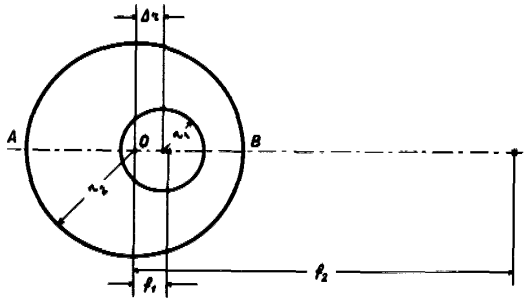

FIGURE 23.2. Cross section of an asymmetrical capacitor.

The distances f_1 and f_2 are defined by

$$\left.\begin{aligned} f_1 f_2 &= r_2^2 \\ (f_1 - \Delta r)(f_2 - \Delta r) &= r_1^2 \end{aligned}\right\}. \qquad (23.1)$$

In the first approximation f_1 and f_2 are expressed in simple fashion by

$$f_1 = \frac{r_2^2}{r_2^2 - r_1^2}\,\Delta r, \qquad (23.2)$$

$$f_2 = \frac{r_2^2 - r_1^2}{\Delta r}. \qquad (23.3)$$

Consider the field along the line OA (Figure 23.2). The distance from the axis O of the outer plate will be denoted by r. The field strength is given by

$$E = 2Q\left(\frac{1}{r + f_1} - \frac{1}{r + f_2}\right). \qquad (23.4)$$

where Q is the charge per unit length of the capacitor. Taking into account expressions (23.2) and (23.3), and neglecting second-order small quantities, we obtain

$$E = \frac{2Q}{r\left[1 + \frac{r^2 + r_2^2}{r\left(r_2^2 - r_1^2\right)}\Delta r\right]} \tag{23.5}$$

The apparent mobility of an air ion is inversely proportional to the time t required for the air ion to pass from one plate to the other. If no radial components of the air-flow velocity occur, then

$$t = \int_{r_1 - \Delta r}^{r_2} \frac{dr}{kE(r)}. \tag{23.6}$$

Calculation yields

$$t = \frac{1}{4kQ}\left\{\left(r_2^2 - r_1^2\right) + \Delta r\left[2r_1 + \frac{2\left(r_2^3 - r_1^3\right)}{3\left(r_2^2 - r_1^2\right)} + \frac{2r_2^2}{r_2 + r_1}\right]\right\}. \tag{23.7}$$

The relative deviation of the apparent mobility from the value at $\Delta r = 0$ is determined by the ratio of the two components in formula (23.7). This ratio is expressed by

$$\delta_k = \frac{8\Delta r\left(r_2^3 - r_1^3\right)}{3\left(r_2^2 - r_1^2\right)^2}. \tag{23.8}$$

It is not difficult to carry out a similar calculation for an air ion moving along the line OB. In this case, the time of passage of the air ion is shortened and the absolute value of the relative deviation of the apparent mobility due to the asymmetry can be determined, in the first approximation, by the same formula (23.8).

For air ions moving in other longitudinal cross sections of the measuring capacitor, the deviation of the apparent mobility will be less than in the above cases. Therefore, formula (23.8) in the first approximation defines the limits of the dispersion of the apparent mobilities resulting from the asymmetry of the measuring capacitor.

The distortion of the flow profile due to the asymmetry causes an additional dispersion of the apparent mobilities. In a flat channel the mean flow velocity at unaltered pressure is proportional to the square of the distance between the walls. Therefore, one can write for the flow across the lines OA and OB

$$\delta_{\bar{u}} < \frac{2\Delta r}{r_2 - r_1}. \tag{23.9}$$

It is readily shown that the error limited by condition (23.9) is always less than the error determined by expression (23.8). Hence, we conclude that the distortion of the flow profile cannot effect more than a twofold increase

in the distortion limits of the mobilities determined by (23.8). In actual fact, the distortion limits of the mobilities increase considerably less.

The problem of asymmetry has special significance in the case of a parallel-plate measuring capacitor. Only an infinitely wide parallel-plate capacitor strictly fulfills the symmetry requirements.

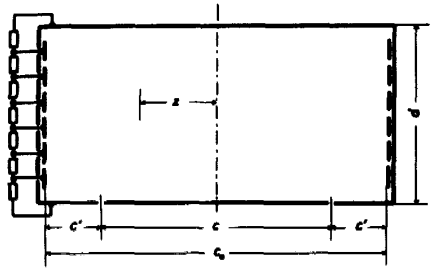

FIGURE 23.3. Cross section of a parallel-plate measuring capacitor.

The electric field of a parallel-plate capacitor may be rendered more homogeneous by means of the method applied in the work /Fontell, 1932/. This method is explained in Figure 23.3.

To prevent distortions it is a prerequisite that the profile of the collector plate is identical in all longitudinal sections of the capacitor. The measuring capacitor should be sufficiently wide so that side walls do not distort the air flow over the collector plates.

In the case of high flow velocity the required distance between the edge of the collector plate and the side wall (Figure 23.3) can be determined on the basis of boundary flow theory. As is well known /Kochin, Kibel, Roze, 1963/, the relative distortion of the flow velocity in the vicinity of the wall is less than 2δ, if the distance from the wall exceeds $\Psi(\delta)\sqrt{\nu x/u_0}$. Some values of the function $\Psi(\delta)$ are listed in Table 23.1.

TABLE 23.1

δ	0.1%	0.2%	0.5%	1%	2%	5%	10%	20%
Ψ	5.7	5.4	4.9	4.5	4.3	3.4	2.7	1.9

According to the above it is sufficient to assume

$$c' = \Psi(\delta)\sqrt{\nu t_0}. \tag{23.10}$$

Independently of the fulfillment of this condition one observes an increase in the flow velocity along the axis of the capacitor, since the widening boundary layer pushes the air toward the center /Yaita, Nitta, 1955/.

At low flow velocities formula (23.10) can yield excessively large values for the distance c', since it does not allow for the effect of the lower and

upper walls. The exact calculation of this effect is only possible for a steady laminar flow. The movement of air ions in a parallel-plate capacitor with a steady laminar flow is treated in the work /Lipscomb, Rubin, Sturdivant, 1947/. We shall use the formula derived in this work for determining the distance x', within which the air ion entering at the edge of the plate is precipitated.

$$x' = \frac{2u_a d^2}{3kU}\left[1 + \frac{32}{\pi^3 \operatorname{ch}\frac{\pi c_0}{2d}}\left(1 + \frac{32}{\pi^3 \operatorname{ch}\frac{\pi c_0}{2d}}\right)\left(1 - \frac{3}{\pi}\operatorname{ch}\frac{\pi z}{d}\right) + \ldots\right]. \qquad (23.11)$$

Here, u_a is the flow velocity in the center of the rectangular channel, c_0 is the width of the channel and z the distance from the central vertical longitudinal cross section (Figure 23.3). In practice, the inequality $c_0/d > 1$ always exists. In the case $z = 0$ the expression in brackets nearly equals unity. For the half-width of the interval of dispersed mobilities we obtain the formula

$$\delta_k \approx \frac{48}{\pi^4 \operatorname{ch}\frac{\pi c_0}{2d}}\left(1 + \frac{32}{\pi^3 \operatorname{ch}\frac{\pi c_0}{2d}}\right)\left[\operatorname{ch}\frac{\pi\left(\frac{c_0}{2} - c'\right)}{d} - 1\right] \qquad (23.12)$$

To simplify calculations, we give in Figure 23.4 curves which enable us to find a satisfactory value for c', when δ_k and c_0/d are known.

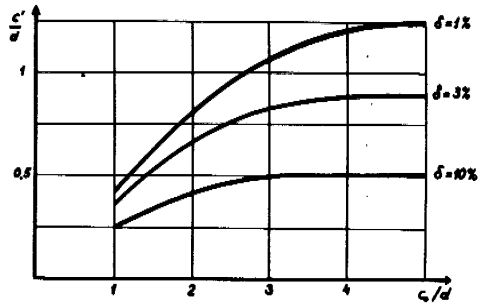

FIGURE 23.4. Curves for finding a satisfactory value for c' at developed laminar flow.

In design calculations of a counter δ_k should be determined in accordance with both formula (23.10) and formula (23.12), and the smaller of the two values selected.

In the case of charged aerosol particles additional distortions may be caused by gravity. The determination of the gravitational effect is quite simple. There exist several different ways for doing this and it is advisable to consider each one separately. For simplicity, we shall assume the flow profile to be uniform in all cases.

In a horizontally oriented cylindrical capacitor the gravitational effect is quite similar to the effect of the asymmetry of the measuring capacitor.

In the first approximation the relative half-width of the interval of dispersed mobilities is given by

$$\delta_k = \frac{2mg\left(r_2^3 - r_1^3\right)\ln\frac{r_2}{r_1}}{3qU\left(r_2^2 - r_1^2\right)}, \qquad (23.13)$$

where m is the mass of the particles.

In a horizontally oriented parallel-plate capacitor the apparent mobilities of air ions of equal mass mobility are not dispersed, but shifted toward one direction. The relative shift is expressed by

$$\delta_k = \frac{mgd}{qU}. \qquad (23.14)$$

In a vertically oriented capacitor the apparent mobilities are also shifted toward one direction. For a cylindrical capacitor we obtain

$$\delta_k = \frac{mg\left(r_2^2 - r_1^2\right)\ln\frac{r_2}{r_1}}{2qUl}, \qquad (23.15)$$

and for a parallel-plate capacitor

$$\delta_k = \frac{mgd^2}{qUl}. \qquad (23.16)$$

Of some interest is the situation in which a parallel-plate capacitor is placed on its side, so that the direction of both the air flow and the electric field are horizontal. In this case distortions are completely eliminated, if the condition

$$c' > \frac{mgd^2}{qU} \qquad (23.17)$$

is fulfilled.

§24. ADSORPTION OF AIR IONS

Gerasimov /Gerasimov, 1941b/ showed that losses of air ions due to adsorption should always be considered when designing inlet devices for an aspiration counter.

Adsorption here applies to the settling of air ions owing to diffusion and attractive electrical image forces. Before calculating the adsorption, we should specify the respective roles of the above two mechanisms.

Consider air ions with mobility k and charge q, distributed uniformly at the initial instant $t = 0$ near the plane conducting wall. If only the diffusion mechanism of adsorption were acting, then in time t as many air ions would settle as are contained in a layer whose thickness equals the mean Brownian displacement of the air ions /Fuks, 1955/. This thickness is given by

$$y_d = \sqrt{\frac{4KTkt}{\pi q}}. \qquad (24.1)$$

When only the image-force mechanism is active, the corresponding layer thickness is

$$y_q = \sqrt[3]{\frac{3qkt}{4}}. \qquad (24.2)$$

The more dominant of the two mechanisms is indicated by the relation

$$\frac{y_d}{y_g} = \sqrt[6]{\frac{1024K^3T^3kt}{9\pi^3 q^5}}. \qquad (24.3)$$

We shall clarify this expression by setting $T = 283°K$:

$$\frac{y_d}{y_q} = 37\sqrt[6]{\frac{k\ (\text{cm}^2/\text{V}\cdot\text{sec})\ t\ (\text{sec})}{[q\ (\text{elem.ch.})]^5}} \qquad (24.4)$$

It appears that in most cases the image-force mechanism of adsorption is of no practical significance. This mechanism may become dominant only for artificially charged aerosol particles. In the following, we shall ignore the image-force mechanism of adsorption.

In the theory of adsorption it is useful to exploit the similarity between the problem at hand and that of heat transfer. The diffusion equation differs from the equation of thermal conductivity only in that the temperature is replaced by the concentration of impurities and that the heat conductivity coefficient is replaced by the diffusion coefficient. The flow of material to the surface where it is adsorbed is proportional to the initial impurity concentration. In calculations, it is convenient to use the ratio Φ_A of these two proportional quantities which we shall call the adsorption flow rate. In analogy to the Newton formula from the theory of heat transfer, we write

$$\Phi_A = \zeta S, \qquad (24.5)$$

where S is the area of the adsorbing surface and ζ is the coefficient of adsorption, which in our case replaces the coefficient of heat transfer.

In order to apply the formulas of heat transfer to problems of adsorption, the specific heat capacity and the density of the material should equal unity, the Prandtl number Pr should be replaced by the Schmidt number $\text{Sc} = \nu/D$ and the Nusselt number Nu by a special adsorption criterion

$$K_A = \frac{\zeta r}{D}, \qquad (24.6)$$

where r is the determining parameter.

Let us first consider the adsorption of air ions when the air is flowing through wire grids. The use of wire grids in the inlet unit presents certain advantages, since with the aid of grids one can screen disturbing electric fields and suppress turbulent pulsations of the incoming flow. The only drawback is that these grids adsorb a certain portion of the air ions.

We assume that the mesh width of the grid is sufficiently wide, so that the adsorption on the grid wires can be compared to that on separate wires.

The heat transfer of a separate wire is described by the empirical equation /Ulsamer, 1932; Gröber, Erk, Grigull, 1958/

$$\text{Nu} = 0.91\ \text{Re}^{0.385}\ \text{Pr}^{0.31}, \qquad (24.7)$$

where the diameter of the wire is taken to be the determining parameter. Formula (24.7) was derived from experimental data for the ranges $0.2 < \text{Re} < 50$ and $6 < \text{Pr} < 1240$, respectively /Davis, 1924/. These values of the Prandtl number correspond to singly charged air ions with mobilities ranging from 0.005 to 1 $\text{cm}^2/\text{volt}\cdot\text{sec}$. The Reynolds number rarely exceeds 50. When $50 < \text{Re} < 10,000$, we should use the formula /Ulsamer, 1932/

$$\text{Nu} = 0.60\ \text{Re}^{0.5}\ \text{Pr}^{0.31}. \qquad (24.8)$$

Formula (24.7), as applied to the problem of air-ion adsorption, becomes

$$\zeta = 0.6\ \frac{u^{0.385} D^{0.69}}{r_0^{0.615} \nu^{0.075}}, \qquad (24.9)$$

where r_0 is the wire radius.

The relative adsorption is determined by the ratio

$$A = \frac{\Phi_A}{\Phi}, \qquad (24.10)$$

where Φ is the air-flow rate.

If a grid is mounted on the inlet of a cylinder of radius r, then that portion of the cross-sectional area covered by wires is given by

$$S = \frac{4\pi^2 r_0 r^2}{h}, \qquad (24.11)$$

where h is the mesh width.

For the relative adsorption we then obtain

$$A = 15\ \frac{r_0^{0.385} r^{1.23} D^{0.69}}{\Phi^{0.615} h \nu^{0.075}}. \qquad (24.12)$$

For normal external conditions

$$A = 0.4\ \frac{[r_0\ (\mu\text{m})]^{0.385} [r(\text{cm})]^{1.23} [k\ (\text{cm}^2/\text{V}\cdot\text{sec})]^{0.69}}{[\Phi(\text{cm}^3/\text{sec})]^{0.615} h(\text{mm})} \qquad (24.13)$$

In the case $ur_0 > 25\nu$, we start with formula (24.8) and obtain

$$A = 0.11\ \frac{[r_0\ (\mu\text{m})]^{0.5} r(\text{cm})\ [k\ (\text{cm}^2/\text{V}\cdot\text{sec})]^{0.69}}{[\Phi(\text{cm}^3/\text{sec})]^{0.5} h(\text{mm})} \qquad (24.14)$$

Formula (24.13) was verified experimentally. The air was ionized with ions of both polarities by the ion generator described in §21. The mean mobility of the air ions was 1.2 $\text{cm}^2/\text{volt}\cdot\text{sec}$. The relative adsorption was determined by comparing the flows obtained in the integral counter with and without a grid. The counter was operated under saturation conditions.

The radius of the outer plate was 0.8 cm. The results are listed in Table 24.1.

The agreement between the experimental data and the calculated values is somewhat rough. However, when designing a counter, formula (24.13) is sufficiently accurate for a preliminary estimation of the errors.

TABLE 24.1

h (mm)	r_0 (μm)	Φ (cm³/sec)	A	
			experimental	(24.13)
0.44	67	220	19%	15%
0.44	67	510	13%	9%
0.44	67	1000	9%	6%
0.785	145	220	10%	11%
0.785	145	510	7%	7%
0.785	145	1000	5%	4%

There exist no suitable empirical formulas in the theory of heat transfer which can be applied here for calculating the adsorption of air ions in the inlet cylinder of the counter. The available formulas /Mikheev, 1956/ apply only to long cylinders. For short cylinders some results are known for the specific case Pr = 0.71. The use of these data in calculating the air-ion adsorption is unjustified for a number of reasons. We shall attempt, therefore, to calculate theoretically the relative adsorption of air ions in the inlet cylinder on the basis of certain simplifying assumptions.

In the work /Siksna, Metnieks, 1953/ this problem is solved under conditions of uniform air flow in the cylinder. Simple calculations yield

$$A = 4\frac{l'^{0.5}}{\Phi^{0.5}}D^{0.5}, \tag{24.15}$$

where l' is the length of the inlet cylinder.

The assumption of a uniform flow profile is somewhat loose, since adsorption takes place in the near-wall layer, where the flow velocity differs considerably from the mean flow velocity. Calculation shows that the layer thickness $Ar/2$, calculated from formula (24.15), is considerably less than the thickness of the boundary layer. According to a preliminary assessment, adsorption takes place completely within the boundary layer where the velocity profile is nearly linear (see formula (18.4)). Accordingly, the following calculations will be carried out on the basis of this assumption.

In still air the adsorption is described by expression (24.1). Hence,

$$\zeta = \frac{2D}{\pi y_d}. \tag{24.16}$$

Here, y_d denotes the equivalent layer thickness from which the air ions are adsorbed. In the boundary layer, ζ is somewhat less than in still air for the same value of y_d. This difference, however, cannot be large. For simplicity, we shall also use (24.16) to describe the adsorption from the boundary layer.

The airflow rate in a layer of thickness y_d is given by

$$\Phi = 0.166\, c y_d^2 \sqrt{\frac{u_0^3}{\nu x}}, \tag{24.17}$$

where c is the width of the strip in question (for the entire tube $c = 2\pi r$) and x is the distance from the beginning of the cylinder. The adsorption flow rate is calculated with the aid of the integral

$$\Phi_A = c\int_0^x \zeta(x')\,dx'. \tag{24.18}$$

Comparing expressions (24.17) and (24.18), we obtain

$$\frac{y_d^2(x)}{\sqrt{x}} = \frac{D}{0{,}83\pi}\sqrt{\frac{\nu}{u_0^3}}\int_0^x \frac{dx'}{y_d(x')}. \tag{24.19}$$

The solution of the above equation is

$$y_d = 1.97\frac{\nu^{1/8}D^{1/3}}{u_0^{1/2}}x^{1/2}. \tag{24.20}$$

Now it is easy to calculate the flow rate Φ_A from formula (24.17) or (24.28). The relative adsorption is given by

$$A = 2.3\frac{l'^{1/2}D^{2/3}}{\Phi^{1/3}\nu^{1/6}}. \tag{24.21}$$

At room temperature and normal pressure we have

$$A = 0.27\frac{[l'(\text{cm})]^{1/2}[k(\text{cm}^2/\text{V}\cdot\text{sec})]^{2/3}}{[\Phi(\text{cm}^3/\text{sec})]^{1/2}} \tag{24.22}$$

The following condition must be fulfilled in order to apply formula (24.12):

$$r \gg \sqrt{\nu t_0'}, \tag{24.23}$$

where t_0' is the filling time of the preliminary cylinder. At the same time it must be ensured that y_d does not exceed the thickness $2\sqrt{\nu t_0'}$, within the limits of which formula (18.4) is sufficiently accurate. The last condition is fulfilled if $Sc > 1$. For normal external conditions it suffices that $k < 6\ \text{cm}^2/\text{volt}\cdot\text{sec}$.

Comparing formulas (24.15) and (24.21), we see that the former gives values which are $1.74\,Sc^{1/6}$ times greater than those of the latter. The error produced upon applying formula (24.16) merely effects a decrease in this ratio. The deviation between formulas (24.15) and (24.12) in the case of the most highly mobile air ions corresponds to a factor of two; for slightly mobile air ions this factor is considerably larger.

In the work /Siksna, Metnieks, 1953/ experimental data are given which coincide well with formula (24.15). This, however, is doubtful, since theoretical considerations speak in favor of formula (24.21).

The controversial character of the problem stimulated further investigation. The methods employed in the relevant experiments were generally the same as those described in the work /Siksna, Metnieks, 1953/. It should be noted, however, that these methods are not fully free from external distorting influences, and do not guarantee high accuracy. A slightly modified version of the setup shown in Figure 15.1 was used. Air ions were generated not by radioactive irradiation but by corona discharge. The ionization was unipolar positive. The mean air-ion mobility $\bar{k} = 1.2\ cm^2/volt \cdot sec$ was determined by the integral counter method with the aid of the same arrangement. The cylinder connected to the electrometer had an inner radius of 0.845cm and a length of 4.0 cm. It was possible to lengthen the cylinder by an additional cylindrical segment of the same radius and of length 8.0 cm. Before measuring the adsorbed flow, the inner plate was removed.

The experimental results presented in Table 24.2 clearly speak in favor of formula (24.21). At large Reynolds numbers the experimental data deviate sharply from the calculated ones (this may be due to turbulence).

The problem of air-ion adsorption from the turbulent flow is more complex and precludes a simple theoretical approach. The use of empirical formulas of the theory of heat transfer to calculate the turbulent adsorption is unjustified, since owing to the extremely short time intervals the image-force mechanism of air-ion capture can no longer be neglected. The adsorption of aerosol particles from the turbulent flow in the measuring capacitor of a counter was estimated in the work /Zachek, 1964b/.

TABLE 24.2

l' (cm)	Φ ($\frac{cm^3}{sec}$)	$Re = \frac{\bar{u}r}{\nu}$	ϱ_+ $\frac{elem.ch.}{cm^3}$	A		
				experimental	(24.21)	(24.15)
4	137	340	20,000	4%	5%	12%
4	257	640	30,000	3%	4%	9%
4	372	930	30,000	3%	3%	7%
4	1010	2500	40,000	6%	2%	4%
4	1790	4500	40,000	5%	1.5%	3%
12	96	240	20,000	13%	11%	25%
12	220	550	30,000	7%	7%	16%
12	416	1040	40,000	6%	5%	12%
12	1010	2500	40,000	8%	3%	8%
12	1750	4400	40,000	7%	2.5%	6%

The adsorption changes the spatial distribution of air ions over the entrance cross section of the measuring capacitor. Therefore, air-ion adsorption in the inlet cylinder is not only manifested in the measurement results of the polar charge densities, but also in the results of the spectral distribution analysis. Counters with inner and outer collector plates behave differently with respect to adsorption. The effect of adsorption on the function G of the integral counter is shown in Figure 24.1. The measurement results of the conductivity are distorted only in the case of the outer collector plate. However, connecting a counter with an outer collector plate has the advantage that the air-ion adsorption in the inlet cylinder does not affect the measurement results of the spectral distribution. In the case of an inner collector plate, the usual methods of data processing give a distorted apparent spectral distribution. In this case the mobilities not only exhibit dispersion but the mean mobility undergoes a shift as well. The relative decrease in the mean mobility equals the relative adsorption A. The dispersion limits of the apparent mobilities are in effect also limited by the value A.

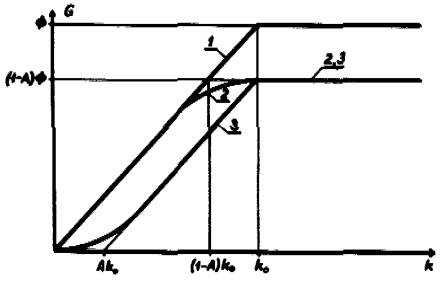

FIGURE 24.1. Function G of an integral counter:

1—in the absence of adsorption; 2—for an inner collector plate; 3—for an outer collector plate.

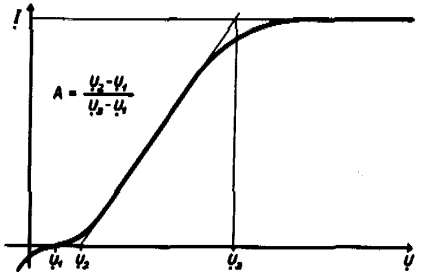

FIGURE 24.2. Determination of the relative adsorption from the characteristics of an integral counter with an outer collector plate:

U_1 — contact potential.

A plot of the function G in the case of an outer collector plate enabled us to determine the relative adsorption A from the experimental curve $I = I(U)$. The essential feature of the suggested method is clearly illustrated in Figure 24.2. This method is in some respects more appropriate than the method of measuring the adsorbed flow of unipolar air ions, and can be recommended for further experimental work on the study of the adsorption of air ions in the inlet cylinder.